



## Calhoun: The NPS Institutional Archive DSpace Repository

---

Theses and Dissertations

Thesis and Dissertation Collection

---

1978-06

### Electroexcitation of giant resonances between 4 MeV and 48 MeV excitation energy in $^{140}\text{Ce}$

Hass, Hubert

Monterey, California. Naval Postgraduate School

---

<http://hdl.handle.net/10945/18420>

*Downloaded from NPS Archive: Calhoun*



Calhoun is a project of the Dudley Knox Library at NPS, furthering the precepts and goals of open government and government transparency. All information contained herein has been approved for release by the NPS Public Affairs Officer.

Dudley Knox Library / Naval Postgraduate School  
411 Dyer Road / 1 University Circle  
Monterey, California USA 93943

<http://www.nps.edu/library>

ELECTROEXCITATION OF GIANT RESONANCES  
BETWEEN 4 MeV AND 48 MeV  
EXCITATION ENERGY IN  $^{140}\text{Ce}$ .

Hubert Hass

# NAVAL POSTGRADUATE SCHOOL

## Monterey, California



# THESIS

ELECTROEXCITATION OF GIANT RESONANCES  
BETWEEN 4 MeV AND 48 MeV  
EXCITATION ENERGY IN  $^{140}\text{Ce}$

by

Hubert Hass

and

Daniel Harry Meyer

June 1978

Thesis  
Co-Advisors:

F.R. Buskirk  
R. Pittman

Approved for public release; distribution unlimited.

T183649

## UNCLASSIFIED

SECURITY CLASSIFICATION OF THIS PAGE (When Data Entered)

REPORT DOCUMENTATION PAGE		READ INSTRUCTIONS BEFORE COMPLETING FORM
1. REPORT NUMBER	2. GOVT ACCESSION NO.	3. RECIPIENT'S CATALOG NUMBER
4. TITLE (and Subtitle) Electroexcitation of Giant Resonances Between 4 MeV and 48 MeV Excitation Energy in $^{140}\text{Ce}$		5. TYPE OF REPORT & PERIOD COVERED Master's Thesis; June 1978
7. AUTHOR(s) Hubert Hass Daniel Harry Meyer		6. PERFORMING ORG. REPORT NUMBER
9. PERFORMING ORGANIZATION NAME AND ADDRESS Naval Postgraduate School Monterey, California 93940		10. PROGRAM ELEMENT, PROJECT, TASK AREA & WORK UNIT NUMBERS
11. CONTROLLING OFFICE NAME AND ADDRESS Naval Postgraduate School Monterey, California 93940		12. REPORT DATE June 1978
		13. NUMBER OF PAGES 71
14. MONITORING AGENCY NAME & ADDRESS (if different from Controlling Office)		15. SECURITY CLASS. (of this report) Unclassified
		15a. DECLASSIFICATION/DOWNGRADING SCHEDULE
16. DISTRIBUTION STATEMENT (of this Report)  Approved for public release; distribution unlimited.		
17. DISTRIBUTION STATEMENT (of the abstract entered in Block 20, if different from Report)		
18. SUPPLEMENTARY NOTES		
19. KEY WORDS (Continue on reverse side if necessary and identify by block number) Electroexcitation of $^{140}\text{Ce}$ Giant Resonances		
20. ABSTRACT (Continue on reverse side if necessary and identify by block number) Electroexcitation of $^{140}\text{Ce}$ was studied using 92 MeV electrons at scattering angles of $90^\circ$ and $105^\circ$ , and 80 MeV electrons at $90^\circ$ . An analysis was made using DWBA calculations and the hydrodynamic model. Among the Giant Resonances found were the GDR at $E_x = 15.3$ MeV ( $\Gamma = 4.4$ MeV), exhausting 122% of the EWSR		

## UNCLASSIFIED

~~SECURITY CLASSIFICATION OF THIS PAGE(When Data Entered)~~

## (20. ABSTRACT Continued)

in the mixed model of Myers, Swiatecki et al.; the isoscalar GQR at  $E_x = 12$  MeV ( $\Gamma = 2.8$  MeV, 50% EWSR); the isovector GQR at  $E_x = 25$  MeV ( $\Gamma = 6.5$  MeV, 41% EWSR in the mixed model); the  $1\hbar\omega_0$  and  $3\hbar\omega_0$  isoscalar GOR's at  $E_x = 6.0$  MeV ( $\Gamma = 1.7$  MeV, 19% EWSR) and at  $E_x = 22.0$  MeV ( $\Gamma = 4.8$  MeV, 19% EWSR); and the  $3\hbar\omega_0$  isovector GOR at  $E_x = 37.5$  MeV ( $\Gamma = 8.5$  MeV, 75% EWSR). The results agree with previous experiments in cerium and other nuclei and, generally, with the calculations of Bohr and Mottelson, Hamamoto, and Liu and Brown. The  $\Delta T$  assignments were based on microscopic and macroscopic considerations.

Approved for public release; distribution unlimited.

Electroexcitation of Giant Resonances  
Between 4 MeV and 48 MeV  
Excitation Energy in  $^{140}\text{Ce}$

by

Hubert Hass  
Lieutenant Commander, Federal German Navy

and

Daniel Harry Meyer  
Lieutenant, United States Navy  
B.S., United States Naval Academy, 1972

Submitted in partial fulfillment of the  
requirements for the degree of

MASTER OF SCIENCE IN PHYSICS

from the

NAVAL POSTGRADUATE SCHOOL

June 1978

ABSTRACT

Electroexcitation of  $^{140}\text{Ce}$  was studied using 92 MeV electrons at scattering angles of  $90^\circ$  and  $105^\circ$ , and 80 MeV electrons at  $90^\circ$ . An analysis was made using DWBA calculations and the hydrodynamic model. Among the Giant Resonances found were the GDR at  $E_x = 15.3$  MeV ( $\Gamma = 4.4$  MeV), exhausting 122% of the EWSR in the mixed model of Myers, Swiatecki et al.; the isoscalar GQR at  $E_x = 12$  MeV ( $\Gamma = 2.8$  MeV, 50% EWSR); the isovector GQR at  $E_x = 25$  MeV ( $\Gamma = 6.5$  MeV, 41% EWSR in the mixed model); the  $1\hbar\omega_0$  and  $3\hbar\omega_0$  isoscalar GOR's at  $E_x = 6.0$  MeV ( $\Gamma = 1.7$  MeV, 19% EWSR) and at  $E_x = 22.0$  MeV ( $\Gamma = 4.8$  MeV, 19% EWSR); and the  $3\hbar\omega_0$  isovector GOR at  $E_x = 37.5$  MeV ( $\Gamma = 8.5$  MeV, 75% EWSR). The results agree with previous experiments in cerium and other nuclei and, generally, with the calculations of Bohr and Mottelson, Hamamoto, and Liu and Brown. The  $\Delta T$  assignments were based on microscopic and macroscopic considerations.

## TABLE OF CONTENTS

I.	INTRODUCTION -----	10
II.	EXPERIMENTAL DETAILS -----	11
III.	THEORY -----	13
	A. ELECTRON SCATTERING -----	13
	B. NUCLEAR MODELS -----	16
	1. Microscopic Model -----	16
	2. Macroscopic Models -----	18
	C. SUM RULES -----	22
	D. QUASI-ELASTIC SCATTERING -----	23
IV.	ACQUISITION AND EVALUATION OF DATA -----	26
	A. DATA COLLECTION -----	26
	B. FITTING PROCEDURE -----	27
	C. ERRORS -----	31
V.	DISCUSSION OF RESULTS -----	32
	A. GENERAL -----	32
	B. THE GIANT DIPOLE RESONANCE (GDR) -----	32
	C. THE ISOSCALAR GIANT QUADRUPOLE RESONANCE (GQR) -----	34
	D. THE ISOVECTOR GIANT QUADRUPOLE RESONANCE (GQR) -----	36
	E. THE GIANT OCTUPOLE RESONANCES (GOR) -----	39
	1. General -----	39
	2. The Isoscalar Giant Octupole Resonances -	39
	3. The Isovector Giant Octupole Resonances -	40
	F. OTHER RESONANCES -----	42

VI. CONCLUSIONS -----	44
LIST OF REFERENCES -----	68
INITIAL DISTRIBUTION LIST -----	71

LIST OF TABLES

I.	Interpolation for $^{140}\text{Ce}$ of the Calculations of Liu and Brown for $^{208}\text{Pb}$ and $^{90}\text{Zr}$ -----	46
II.	Experimental Parameters -----	47
III.	Data Analysis Results -----	48
IV.	Giant Resonances -----	49

## LIST OF FIGURES

1.	Inelastic $^{140}\text{Ce}$ spectrum with and without background -----	51
2.	Inelastic $^{140}\text{Ce}$ spectra with background -----	52
3.	Inelastic $^{140}\text{Ce}$ spectra without background -----	53
4.	Photon absorption cross section of $^{140}\text{Ce}$ -----	54
5.	Comparison of DWBA cross sections for E1 to E4 transitions divided by the Mott cross sections -----	55
6.	Comparison of the DWBA and experimental form factors for the resonance found at 15.3 MeV -----	56
7.	Comparison of the difference between the experimental form factor and the Goldhaber-Teller model and the DWBA form factors for the resonance found at 15.3 MeV -----	57
8.	Comparison of the DWBA and experimental form factors for the resonance found at 12.0 MeV -----	58
9.	Comparison of the difference between the experimental and the DWBA form factors for the resonance found at 12.0 MeV -----	59
10.	Comparison of the DWBA and experimental form factors for the resonances found at 6.0, 7.4, and 10.0 MeV -----	60
11.	Comparison of the DWBA and experimental form factors for the resonances found at 22.0, 25.0, 31.0 and 37.5 MeV -----	61
12.	Comparison of the difference between the experimental and the DWBA form factors for the resonance found at 25.0 MeV -----	62

## ACKNOWLEDGMENTS

We are greatly indebted to our thesis advisors, Professors F.R. Buskirk and R. Pitthan. Prof. Buskirk guided us through the gulches of theoretical nuclear physics, introduced us to the complexity of the LINAC, and always helped us instantly to overcome difficulties during our experiments, no matter what the hour was. Prof. Pitthan's total commitment to research, his permanent help, encouragement and constructive criticism made it possible to evaluate the data and create a meaningful work.

We also want to express our thanks to Professor J.N. Dyer, who taught us relativistic quantum mechanics in such an enjoyable way and was always ready to help us run the LINAC.

Special thanks go to Mr. H. McFarland and Mr. D. Snyder for keeping the LINAC operational at all times, and to E. Hunter and G. Pozinsky for equally sharing the watches with us while we conducted the experiments.

Finally we thank our wives, who never lost patience while this work was prepared, not even during the endless hours of data taking.

## I. INTRODUCTION

It was not until about 1970 that inelastic electron scattering was successful in locating and determining giant multipole resonances in medium and heavy nuclei. Pitthan and Walcher (PitW 71) (Pit 73) experimented with 50 and 65 MeV electrons, using  $^{140}\text{Ce}$ ,  $^{139}\text{La}$ , and  $^{141}\text{Pr}$  as targets. They found in  $^{140}\text{Ce}$  low lying states (0 to 3 MeV) and three giant resonances at 8.7, 12.0, and 15.3 MeV, which were identified as M1, E2 ( $\Delta T = 0$ ) and E1 transitions respectively. Besides these, resonances appeared at 10 and 25 MeV, the latter one thought to be the isovector E2 giant resonance.

To investigate further the spherical nucleus,  $^{140}\text{Ce}$ , which has a closed neutron shell ( $N = 82$ ), it was decided to extend the previous work using higher beam energies (80 and 90 MeV), higher momentum transfer (up to  $0.75 \text{ fm}^{-1}$ ), an extended range of excitation energy (up to 48 MeV), and scattering angles no greater than  $105^\circ$ , thus deemphasizing transverse transitions.  $^{140}\text{Ce}$  was chosen because the resonances of the continuum have been found to be relatively narrow, thus allowing separation of overlapping states by a line shape fit. Special emphasis was put on the investigation of the giant dipole resonance at 15.3 MeV because of contradicting reports on the existence of a monopole resonance in the same energy region, and on other isovector resonances which have been investigated mainly with  $(e, e')$ .

## II. EXPERIMENTAL DETAILS

The NPS 120 MeV linear accelerator which was used for the experiments has been described by Pitthan, et al. (PitB 77). The target for all experiments was natural cerium obtained from the Ventron Corporation. The metal was rolled to a self-supporting foil of thickness  $126 \text{ mg/cm}^2$ , which was quickly put under high vacuum in the target chamber to avoid oxidation.

Three spectra were collected. One at an incident beam energy of 79.6 MeV and a scattering angle of  $90^\circ$ , measuring the inelastic spectrum from 77 to 27 MeV, one at 92.1 MeV and  $90^\circ$ , measuring the inelastic spectrum from 88 to 40 MeV, and one at 92.8 MeV and  $105^\circ$ , measuring the inelastic spectrum from 88 to 40 MeV. The last spectrum was measured twice and added, since with higher momentum transfer the cross section becomes smaller. This causes a long duration of the experiment to accumulate enough counts for good statistical accuracy (approximately two weeks of beam time), during which any breakdown of the accelerator would impede the reliability of the measurements, especially above 25 MeV excitation energy.

The variation of elastic momentum transfer,  $q$ , in this work (from 0.57 to  $0.75 \text{ fm}^{-1}$ ) was thought to be sufficient to investigate most of the resonances, because together with the original data from Pitthan ( $0.37$  to  $0.47 \text{ fm}^{-1}$ ), this

momentum transfer range was thought to be sufficient to identify existing resonances. It was later discovered that an experiment at even higher  $q$  might have been useful to identify resonances at higher excitation energies. However, time did not permit such an experiment.

Forward angles were chosen for the experiments to emphasize longitudinal electric transitions.

A list of experimental parameters is given in Table II.

### III. THEORY

#### A. ELECTRON SCATTERING

The angular distribution of scattered electrons is affected by size and shape of the nuclear charge distribution. The finite size of the nuclear charge density gives rise to deviations from the Mott cross section, and the nuclear charge distribution can be studied by measuring these deviations. By scattering electrons elastically, the ground-state charge distribution may be investigated. In the plain wave Born approximation (PWBA) the nuclear cross section, neglecting recoil, becomes

$$\frac{d\sigma}{d\Omega} = \left( \frac{d\sigma}{d\Omega} \right)_{\text{Mott}} |F_{el}(q)|^2$$

where

$$\left( \frac{d\sigma}{d\Omega} \right)_{\text{Mott}} = \frac{z^2 e^4}{4E_i^2} \frac{\cos^2 \frac{\theta}{2}}{\sin^4 \frac{\theta}{2}},$$

$E_i$  is the incident electron energy,

$$F_{el}(q) = \int \rho(r) e^{-iq \cdot r} dr$$

is called the form factor, and

$$q = (k_1^2 + k_2^2 - 2k_1 k_2 \cos \theta)^{1/2}$$

is the momentum transfer, where  $k_1$  and  $k_2$  are the incident and scattered electron momentum respectively, and  $\theta$  is the scattering angle. For incident and scattered electron energies that are much greater than the electron rest mass,  $m_0 c^2 = .5109$  MeV, the momentum transfer simplifies to

$$q^2 \approx 4k_1 k_2 \sin^2 \frac{\theta}{2} .$$

Since the Mott cross section describes scattering of relativistic electrons from a point charge, the information concerning the charge distribution is contained within the form factor,  $F(q)$ .

Investigation through inelastic scattering may reveal multipolarities of the various inelastic transitions excited by the electron. A collective excitation involving transitions over the same number of main shells of a nucleus, but various subshells, is called a giant resonance and can be studied with inelastically scattered electrons.

In PWBA the differential cross section for nuclear excitations by inelastic electron scattering is

$$\left(\frac{d\sigma}{d\Omega}\right)_{PWBA} = \sum_{\lambda} \left(\frac{d\sigma}{d\Omega}\right)_{e\lambda} + \sum_{\lambda} \left(\frac{d\sigma}{d\Omega}\right)_{m\lambda}$$

which is the sum over the cross sections for electric and magnetic multipole transitions (The 72). PWBA is inadequate,

however, for heavy nuclei, since it does not take into account the distortion of the incoming and outgoing electron waves by the Coulomb potential of the nucleus. A better approximation than PWBA is DWBA (distorted wave Born approximation). In this method one solves the Dirac equation for the relativistic electron, taking into account the effect of the nuclear charge distribution on the electron wave functions, and uses these distorted waves to calculate the interaction cross section.

For low  $q$  elastic scattering only one parameter, namely the rms radius, can be extracted to give an indication of the charge distribution in the ground state. The rms radius is related to the second radial moment of the charge distribution. As  $q$  is increased, higher moments may be extracted. For inelastic scattering producing multipole excitations the  $\lambda^{\text{th}}$  radial moment of the charge density defines the reduced transition probability,  $B(E\lambda)$ :

$$B(E\lambda) = (2\lambda+1) \left| \int r^\lambda \rho_{tr}(r) r^2 dr \right|^2 .$$

The transition radius,  $R_{tr}$ , is related to both the  $\lambda^{\text{th}}$  and  $\lambda+2^{\text{th}}$  radial moment:

$$R_{tr}^2 = \frac{\int r^{\lambda+2} \rho_{tr}(r) r^2 dr}{\int r^\lambda \rho_{tr}(r) r^2 dr} .$$

Extraction of the moments can be done model independently only in PWBA. In heavier nuclei DWBA has to be used and

results are no longer model-independent, thus making the decomposition of the form factor into moments no longer useful.

DWBA calculations take into account the effects of finite excitation energy and include both transverse electric and longitudinal electric contributions. However in the hydrodynamic (Tassie) model, for example, the transverse contributions are due only to contributions from the convection current (continuity equation) and are small when the scattering angle is smaller than  $150^\circ$ . Five conditions are assumed in DWBA analysis: (1) The transition is that of an electric multipole; (2) the ground state is spherically symmetric; (3) the nuclear recoil energy is negligible compared to the excitation energy; (4) the interaction involved is free of polarization or dispersion effects; (5) the excited-state charge distribution is not significantly distorted from that of the ground state (ZieP 68).

## B. NUCLEAR MODELS

### 1. Microscopic Model

Assuming that the individual nucleons move independently, nuclei can be described by a shell model, similar to atoms. An interaction of an electron with a nucleus can cause a nucleon to leave its shell, going into a higher one and leaving a hole behind. If the incoming electron has sufficient energy, the nucleon may be totally removed from the nucleus. Individual single particle states caused

by these transitions are weak and cannot generally be seen above particle threshold, since the final states are broadened because they are particle unstable. Collective states, however, involving many single particle transitions, may be strong enough to rise sufficiently above the background to be seen. Of these collective states the giant dipole resonance (GDR), E<sub>1</sub>, is the most thoroughly investigated. It represents a transition over one main shell ( $1\hbar\omega_0$ ) in the shell model. This resonance is predominantly excited by photons, where the cross section can be measured very accurately (Ber 76). A measurement of the giant resonance region in <sup>140</sup>Ce is shown in Figure 4.

Assuming the excited nucleon makes an E2 transition (giant quadrupole resonance), the energy of the resulting resonance in the shell model should be  $2\hbar\omega_0$ . Since more than one nucleon can be excited at the same time, parts of the shell are empty and a distorted potential is produced. Bohr and Mottelson (BohM 75) found that this lowers the resonance energy by  $\sqrt{2}$ , which gives for the isoscalar ( $\Delta T = 0$ ) GQR

$$E_x = \sqrt{2} \hbar \omega_0 \approx 58 A^{-1/3} \text{ MeV}$$

where A is the atomic number. For the isovector ( $\Delta T = 1$ ) GQR they found

$$E_x = 130 A^{-1/3} \text{ MeV} .$$

For the giant octupole resonance (GOR), E3,  $1\hbar\omega_0$  and  $3\hbar\omega_0$  transitions are allowed in the shell model. Octupole resonances found at lower excitation energies are generally considered to be of isoscalar nature, whereas those found at higher energies can be expected to be iso-vector transitions. This can be explained by the particle-hole interaction, which is attractive for isoscalar and repulsive for isovector states. Hamamoto, in a schematic random phase approximation (RPA) calculation on the basis of Bohr and Mottelson's model, predicts isoscalar E3 resonances at  $25 \text{ A}^{-1/3} \text{ MeV}$  ( $1\hbar\omega_0$ ) and  $106 \text{ A}^{-1/3} \text{ MeV}$  ( $3\hbar\omega_0$ ). The corresponding isovector states are at  $53 \text{ A}^{-1/3}$  and  $195 \text{ A}^{-1/3} \text{ MeV}$ . In the meantime, more detailed calculations have been performed by a variety of authors (BorK 75, KreS 74), the most detailed being those of Liu and Brown (LiuB 76), who have calculated giant resonances in the spherical nuclei  $^{16}\text{O}$ ,  $^{40}\text{Ca}$ ,  $^{90}\text{Zr}$ , and  $^{208}\text{Pb}$  using large configuration spaces in the random phase approximation based on the Hartree-Fock ground states of a newly developed Skyrme interaction. They found reasonable agreement with many experiments. This work will compare the experimental results with the calculations of Liu and Brown, using an interpolation of their results for  $^{90}\text{Zr}$  and  $^{208}\text{Pb}$  (Table I).

## 2. Macroscopic Models

Over the years considerable effort has been undertaken to describe the GDR using a macroscopic model. In

1948 Goldhaber and Teller (Golt 48) proposed three alternative models:

a) The force which displaces a proton from its average position in the nucleus is proportional to the displacement. The force does not differ for different nuclei and different protons in the nucleus, thus placing the GDR at the same excitation energy for every nucleus, a result which is obviously wrong.

b) The neutrons and protons form two separate fluids, staying within a common surface. When the nucleus is excited, these fluids interpenetrate each other. The excitation energy of the GDR depends on the square root of the restoring force and is thus proportional to  $A^{-1/3}$ . This model had been proposed previously by Migdal (Mig 44), who gives the expression  $E_x = 23.7 A^{-1/3} \sqrt{\beta Z/A}$  for the average energy of the dipole mode, with  $\beta$  the coefficient of the symmetry term  $\beta(N-Z)^2/A$  in the semiempirical Bethe-Weizsäcker mass formula. In 1950 Steinwedel and Jensen refined this model (SteJ 50) and found  $E_x = 80 A^{-1/3}$  MeV. The transition charge density from this model is

$$\rho_{tr}^{SJ}(r) = C_{SJ} j_1(qr/c) \rho_0(r) .$$

c) Neutrons and protons again form separate fluids. This time, however, each fluid has a rigid surface and the resonance results from the harmonic oscillations of the two

density distributions with respect to each other. The restoring force is proportional to the surface area and the excitation energy is proportional to  $A^{-1/6}$ . The ground state charge density,  $\rho_o(r)$ , can be assumed to be rigidly displaced resulting in a total charge density of

$$\rho_o(r) - \rho(r) = \frac{1}{2} \vec{d} \cdot \nabla \rho_o(r) ,$$

where  $\vec{d}$  is the displacement vector between the centers of the proton and neutron distributions. The transition charge density becomes

$$\rho_{tr}^{GT}(r) = C_{GT} r^{\lambda-1} \frac{d\rho_o(r)}{dr} ,$$

where  $\lambda$  is the multipolarity. This equation is equal to the Tassie hydrodynamic model of nuclear shape oscillations (Tas 56).

In 1977 Myers, et al. (MyeS 77) discussed two new features for the GDR. They calculated the restoring forces in terms of the droplet model (MyeS 69) (MyeS 73) (Mye 74) and found the GDR motion to be a superposition of the flow of the Goldhaber-Teller (GT) and Steinwedel-Jensen (SJ) models with the relative magnitudes of the two models determined by the coupling between them and the associated forces and inertias. Their results show that the GDR is essentially a GT mode for light nuclei with an increasing admixture of

the SJ mode for heavier nuclei. The dependence of the excitation energy on the atomic number was found to be intermediate between that of the GT and SJ modes, namely  $E_x \sim A^{-0.23}$ .

To calculate the elastic and inelastic cross sections for all resonances in this work, a Fermi charge distribution of

$$\rho_0(r) = N_0 \left(1 + \exp \frac{r - c}{t/4.40}\right)^{-1}$$

was assumed for the ground state, where  $N_0$  is the normalization charge density,  $c$  is the half density radius,  $t$  is the skin thickness and  $r$  is the radial coordinate. The skin thickness is measured as the distance between the points where the charge density is 90% and 10% of the values at the origin.

The values  $c = 5.78$  and  $t = 2.31$  fm were used for natural cerium (Tho 69). Ziegler and Petersen (ZieP 68) parameterized the transition probability using  $c$  and  $t$  by taking the transition charge density to be the derivative of a fictitious charge distribution described by  $c_{tr}$  and  $t_{tr}$ . In the hydrodynamic (Tassie) model  $c = c_{tr}$  and  $t = t_{tr}$ . These parameters were used for the calculation of the inelastic cross sections throughout this work, except where noted. The program used for the inelastic cross sections is that of Tuan et al. (TuaW 68). The elastic cross sections

were calculated with the phase shift program of Fischer and Rawitscher (FisR 64).

### C. SUM RULES

Sum rules provide a means for predicting the total expected strength of excitations. If the theoretical transition probability for an electron induced transition is summed over all final nuclear states of any possible angular momentum and isospin, the final states may be removed using closure, and the result depends only on the ground state properties (WarW 69). One should keep in mind, however, that sum rules are only a rough upper limit, and that they especially may be exceeded for isovector excitations (BohM 75). For this work the following formulas were used (PitB 74):

$$B(E\lambda)_{SPU} = \frac{(2\lambda+1)}{4\pi} \left( \frac{3R_0}{\lambda+3} \right)^2, \quad R_0 = 1.2 A^{-1/3}$$

$$S(E\lambda, \lambda > 1) = E_x B(E\lambda) = \frac{Z\lambda(2\lambda+1)^2 h^2}{8\pi M} \left\langle R^{2\lambda-2} \right\rangle_0$$

$$\Gamma_\gamma^\circ = \frac{8\pi\alpha}{[(2\lambda+1)!!]^2} \frac{\lambda+1}{\lambda} \frac{E_x^{2\lambda+1}}{(\hbar c)^{2\lambda}} \frac{B(E\lambda)}{(2\lambda+1)}$$

$$S(E1) = E_x B(E1) = \frac{g\hbar^2}{8\pi M} \frac{NZ}{A}$$

$$S(E0) = E_x |M_{fi}|^2 = \frac{\hbar^2}{M} A \left\langle R^2 \right\rangle_0$$

The  $E_1$  sum rule is the isovector sum rule, because no isoscalar dipole excitation exists in first order (center of mass motion); the other sums are divided into  $\Delta T = 0$  and  $\Delta T = 1$  parts by assigning  $Z/A$  and  $N/A$  fractions of the total sum.

#### D. QUASI-ELASTIC SCATTERING

If the momentum transfer is high enough, electrons may scatter elastically from individual nucleons within the nucleus. This process is called quasi-elastic scattering. If sufficient momentum is transferred from the incoming electron to the nucleon, the latter may leave the nucleus with some kinetic energy and the energy loss of the electron may result in a measurable quasi-elastic peak.

The inelastic electron-nucleus cross section has been calculated with the Fermi gas model in the quasi-elastic region by Moniz (Mon 69). In the Fermi gas model the electron scatters elastically from a single nucleon with the recoiling nucleon assumed to leave the Fermi sphere. The Pauli exclusion principle prohibits the nucleon from scattering into an already occupied state. The final nucleon energy is given by

$$E_{kf} = (k^2 + M^2)^{1/2},$$

where  $k$  is nucleon momentum and  $M$  is the nucleon mass. The initial nucleon energy is

$$E_{ki} = \frac{k^2}{2M} + U(k^2) = \frac{k^2}{2M^*} + U(0) ,$$

where  $M^*$  is the effective mass,

$$M^* = \frac{M}{1.4}$$

(KawK 68), and  $U(k^2)$  is the effective single-particle potential which shifts the electron energy loss,  $\omega$ , to take into account nuclear binding. Moniz treats this potential as a constant,  $\bar{\epsilon}$ , equivalent to the average nucleon interaction energy.

The energy of the quasi-elastic peak will increase with the momentum transfer,  $q$ , and approach the effective free nucleon kinetic energy,  $q^2/2M^*$ , at large values of  $q$ . Moniz, et al. (MonS 71) calculated  $\bar{\epsilon}$  and the nuclear Fermi momentum,  $k_F$ , for a number of elements, from which, through interpolation,  $\bar{\epsilon} = 42$  MeV and  $k_F = 262$  MeV/c were obtained for cerium. To compute the cross section, an energy-conserving delta function is involved (MonS 71), namely

$$S[\omega + (\frac{k^2}{2M}) - \bar{\epsilon} + (\frac{(\vec{k} + \vec{q})^2}{2M})] .$$

This leads to

$$\omega = \bar{\epsilon} + \frac{kq}{M} + \frac{q^2}{2M^*} .$$

At the peak of the quasi-elastic distribution,  $k = 0$   
may be assumed, giving

$$\omega_p = \bar{\epsilon} + \frac{q^2}{2M^*} .$$

The same result is given by Uberall (Ube 71). For the lowest momentum transfer in the experiments for this work ( $0.45 \text{ fm}^{-1}$ ),  $\omega_p = 46.2 \text{ MeV}$ . Thus corrections for quasi-elastic scattering need not be made for the spectra investigated in this work.

Ferlic and Waddell (FerW 74) did the same analysis for their work on  $^{197}\text{Au}$ , but approximated the nucleon momentum  $k$  by the Fermi momentum  $k_F$ . Thus the nucleon momentum became the dominant term in the calculation of  $\omega_p$ , besides  $\bar{\epsilon}$ , which is wrong. They should have calculated  $\omega_p = 47 \text{ MeV}$  instead of 73 MeV for the lowest momentum transfer in their work ( $0.44 \text{ fm}^{-1}$ ).

#### IV. ACQUISITION AND EVALUATION OF DATA

##### A. DATA COLLECTION

Cerium foils served as targets for 92 MeV electrons at scattering angles of 90° and 105° and 79.4 MeV electrons at 90°, as described previously. The targets were positioned to bisect the scattering angle giving a transmission geometry which kept the path length of the scattered electrons constant and at a minimum. The counting system of the NPS linac consists of ten scintillation counters which are linearly arranged in the focal plane of a 16 inch magnetic spectrometer. The arrangement allows the coverage of a 3% momentum (energy) range at one spectrometer setting.

The spectrometer energy was decremented in 0.1 MeV steps. The counts in the 10 counters were recorded on magnetic tape and transferred to the IBM 360/67 computer facility of the NPS. Elastic and inelastic spectra were obtained for all three experiments. The elastic cross sections were determined using the phase-shift code of Fischer and Rawitscher (FisR 64). The inelastic spectra were measured relative to the elastic cross sections and a least square fit program (PitB 77) was used to evaluate them. Bremsstrahlung and Schwinger corrections were applied to the elastic spectra.

## B. FITTING PROCEDURE

A Breit-Wigner type line shape was chosen for all lines in the inelastic spectra since it was found by Gordon and Pitthan (GorP 77) to fit the nuclear strength function for an E1 transition better than Gaussian or Lorentz line forms. The line width for all resonances, which may consist of many unresolved states, especially at energies below 10 MeV, was found to be greater than the line width of the elastic peak. Gordon and Pitthan state further that there are slight but important differences between the shape of the strength function and the cross section. The latter depends on primary energy and scattering angle, whereas the first does not. Thus the resonance energies and widths given later in this work are those of the strength function.

Evaluation of the data in the range between 4 and 8 MeV was considerably complicated by the fact that the spectrometer of the NPS linac causes instrumental scattering (ghost peak) which is found at an excitation energy of approximately 8% of the elastic peak energy and has a constant area of 1.5% of the elastic peak area (HouM 77). The same line shape as that of the elastic peak was assumed for the ghost peak and it was subsequently frozen, i.e., peak height ratio and width were held constant. The ghost peak also does not appear in the spectra shown in Figures 1, 2, and 3.

An exceedingly important part of the analysis of an inelastic spectrum is the evaluation of the background

underlying it. It consists mainly of the so-called elastic radiation tail, caused by photoemission before, during and after the scattering event, by Møller scattering (electron-electron scattering) and by energy straggling and ionization. The radiation calculation of Ginsberg and Pratt (GinP 64) was used for the calculation of radiation during scattering, but with the phase shift calculation of the elastic form factor replacing the original Born approximation form factors. Other components adding to the total background are the general room background and electrons scattered from the target and subsequently from the spectrometer wall. To describe the total background, not including the "ghost peak", a function of the energy of the outgoing electron,  $E_f$ , was chosen:

$$BGR(E_f) = [P_1 + P_2(E_f - E') + P_3 \cdot RT] \exp[P_4 \left( \frac{E_f - E_{el}}{E_f} \right)] ,$$

where  $P_1$  through  $P_4$  are the background fitting parameters,  $E'$  is the energy center of the fitted range,  $E_{el}$  is the energy of the elastic peak, and RT is the radiation tail. The above background was used in all spectra.

Four criteria were considered for placement of a resonance in the inelastic spectrum: (1) Previous observation in  $^{140}\text{Ce}$  by Pitthan in Darmstadt (Pit 73) and observation in similar nuclei like  $^{141}\text{Pr}$ ,  $^{142}\text{Nd}$ ,  $^{144}\text{Sm}$ , and  $^{165}\text{Ho}$ ; (2) the knowledge of resonances found in  $^{140}\text{Ce}$  by photonuclear

experiments (LepB 76); (3) the observation of a peak above the background in the raw spectra; (4) the necessity to add a resonance to achieve a consistent overall fit. In the case of heavy nuclei it is very difficult to see individual resonances in the raw spectra, especially at high excitation energies. Position and half width can almost never be estimated accurately by an eye-ball fit since several collective states may be overlying each other. To be able to see the structure of the giant multipole resonances the background must, therefore, be subtracted from the raw data (Figures 1 and 2).

A first attempt to analyze the inelastic spectra was made by inserting the lines seen previously by Pitthan at 8.6, 10.0, 12.0, 15.3, and 25.0 MeV (Pit 73). For the position and the width of the line at 15.3 MeV the ( $\gamma$ ,n) spectrum shown in Figure 4 (LepB 76) was also considered. Other resonances which had been seen in  $^{208}\text{Pb}$  (PitB 74),  $^{165}\text{Ho}$  (MooB 76) and other nuclei were entered, which gave rise to resonances at 38 and 22 MeV. Finally, lines at 6.0, 7.4, and 30.5 MeV were needed to obtain a reasonable least squares fit ( $\chi^2 < 1$ ).

Once a line was fit, the excitation energy and half width were held constant at the average value and only the peak height of the resonance was allowed to change. In this way a  $\chi^2$  and a transition strength,  $B(E\lambda)$ , were obtained. The transition strength is the ratio of the squares of the

experimental form factor to the theoretical form factor calculated with the DWBA program:

$$B(E\lambda) = \frac{|F(q^2)|_{\text{exp}}^2}{|F(q^2)|_{\text{DWBA}}^2} ,$$

where

$$|F(q^2)|_{\text{exp}}^2 = \left(\frac{A_{\text{in}}}{A_{\text{el}}}\right) \frac{\sigma_{\text{el}}}{\sigma_{\text{Mott}}} ,$$

because the DWBA calculations are normalized to  $B = 1 e^2 \text{ fm}^2$ .

The  $B(E\lambda)$  value was later used to determine the percentage of the energy weighted sum rule (EWSR) exhausted by the resonance found experimentally,

$$\text{EWSR}(\%) = \frac{B(E\lambda) \cdot E_x}{S(\lambda)} .$$

To obtain values of  $E_x$  and  $\Gamma$  for the different lines, various combinations of these parameters were used, all yielding a reasonable  $\chi^2$ . The overall results of the data evaluation are given in Table III. To determine the multipolarity of the different resonances, the experimentally obtained form factors were plotted versus momentum transfer and compared with the curves of theoretical form factors calculated with the DWBA program of Tuan et al. (Tuaw 68). (See Figures 5 through 12.) This resulted in the designation of one or more possible multipolarities for the individual

resonances as well as the assignment of a strength. Although isospin cannot be determined from electron scattering, isoscalar and isovector character was assigned to the stronger lines which were identifiable with main shell transitions, based on microscopic and macroscopic considerations.

#### C. ERRORS

The errors in excitation energy and halfwidth are best estimates from the minimum and maximum values of the parameters which would fit the spectrum while still yielding a  $\chi^2$  of less than 1.0. The error in % EWSR given in the text is based on the standard deviation of the average sum rule exhaustion and is, therefore, more a measure for the fit to a certain model than a measure for the total uncertainty. The total error given in Table IV is based on the maximum and minimum value of the areas under the curves experienced through the fitting procedure.

## V. DISCUSSION OF RESULTS

### A. GENERAL

The three spectra investigated in this work are shown with and without background in Figures 1 to 3. It has to be noted that the background is fairly large in all cases, but decreases as momentum transfer increases. All spectra have very noticeable structure between 4 and 25 MeV. They show less structure and considerable background sensitivity beyond 25 MeV which causes some problem in resonance evaluation in that region, as will be discussed later. After subtraction of the background, the variation of the individual resonances with different momentum transfer can be seen.

The curve fitting results are given in Table III. The multipolarities, half widths and strengths of the transitions which could be determined with little doubt, are given in Table IV. Figures 5 through 12 show the calculated form factor versus momentum transfer along with the form factors obtained experimentally in this work.

### B. THE GIANT DIPOLE RESONANCE

The electric dipole mode for  $^{140}\text{Ce}$  has been accurately measured by ( $\gamma, n$ ) scattering (LepB 76); see Figure 4. An excitation energy  $E_x = 15.04$  MeV, half width  $\Gamma = 4.41$  MeV, and a peak height  $P = 383$  mb, corresponding to an integrated cross section  $A = \frac{\pi}{2} \cdot \Gamma \cdot P = 2653$  MeVmb, were obtained,

from which a transition strength (B-value) of  $43 \text{ fm}^2$  can be derived (GorP 77). The various form factors calculated by the DWBA program using the GT, SJ, and Myers-Swiatecki model were then normalized to  $43 \text{ fm}^2$ .

A resonance was found at  $E_x = 15.3 \pm 0.2 \text{ MeV}$  ( $80 \text{ A}^{-1/3}$ ) with  $\Gamma = 4.4 \pm 0.2 \text{ MeV}$ , believed to be the GDR. Comparing the experimental results of this work, combined with those of Pitthan (Pit 73), with the theoretical form factors mentioned above (Figure 6), revealed that the resonance in question was indeed compatible with the GDR, exhausting  $167 \pm 40\%$  of the sum rule if the GT model was used. However, as can be seen from Figure 6, there is a difference between the experimental variations of the form factor as a function of  $q$  and the GT curve. Taking this difference and plotting it versus  $q$  (Figure 7), shows that an isoscalar monopole transition ( $E0, \Delta T = 0$ ), exhausting approximately 44% of the EWSR, or an  $E2$ , could be lying under the GDR. Similar findings have been presented by Richter (Ric 77) for  $^{142}\text{Nd}$  and  $^{144}\text{Sm}$ , in which he has proposed  $E0$  transitions of 28% and 20% EWSR, respectively. Interpolating the calculations of Liu and Brown (LiuB 76) shows that for  $^{140}\text{Ce}$  an isoscalar  $E0$  should be expected at approximately 18 MeV (34% EWSR).

Figure 6 also shows that in addition to not coinciding with the GT model, the experimental form factors do not fit the SJ model either. A possible explanation was proposed by Myers et al. (MyeS 77), who state that the rigid fixed

spherical cavity of the SJ modes imposes a harsh and unrealistic constraint on the motion of the nucleons. The droplet model (MyeS 69), which explicitly identifies the energy associated with displacing the surface of the neutron distribution from that of the proton distribution, permits a more realistic calculation of the restoring force for the GT mode than the "ad hoc" procedure used in the original work. Myers et al. realized that a much more satisfactory macroscopic description of the GDR results, in which the GDR is found to be a superposition of GT and SJ modes, as described previously under "nuclear models". For an atomic mass number of 140, Myers et al. calculated the ratio of the SJ component to the GT component to be 0.76 (see MyeS 77). Again DWBA form factors were calculated using this model and Figure 6 shows that the results agree well with the new model, where the resonance exhausts  $122 \pm 12\%$  EWSR. It, therefore, remains unanswered whether an E0 transition really exists under the E1, or whether the models used thus far are not adequate to describe the motion of the neutrons and protons within the nucleus. If the Myers et al. fits to the droplet mode are correct, their results might also apply to higher order isovector transitions.

### C. THE ISOSCALAR GIANT QUADRUPOLE RESONANCE

Figure 8 shows that the resonance found at  $E_x = 12.0 \pm 0.2$  MeV with  $\Gamma = 2.8 \pm 0.2$  MeV conforms to an E2 form factor

curve. It dissipates  $63 \pm 17\%$  EWSR assuming a pure ( $c_{tr} = 1.0$  c) GT model. It was observed, however, that the experimental form factors deviate in a consistent manner from the GT curve. There are two possible explanations for this deviation. First, it was assumed that a higher multipolarity was underlying the E2. By again taking the differences between the results and the theoretical E2 form factors (the form factor obtained in the 50 MeV/93° experiment by Pitthan (Pit 73) was assumed to coincide with the theoretical value for this purpose), it was found that a higher multipolarity, most likely an E3 (see Fig. 9), may indeed exist under the E2. This octupole transition exhausts roughly 8% of the isovector EWSR. Secondly, by changing the parameterized half density radius to  $c_{tr} = 0.95$  c, it was found that the theoretical form factors were in much better agreement with those obtained experimentally. In this case the E2 strength drops to  $50 \pm 5\%$  EWSR.

Youngblood et al. (YouR 77) performed  $\alpha$ -scattering experiments on  $^{144}\text{Sm}$  and  $^{208}\text{Pb}$  and reported an isoscalar E2 state at 63 and  $65 \text{ A}^{-1/3}$  MeV, respectively. The one found in  $^{144}\text{Sm}$  had an excitation energy of  $12.4 \pm 0.4$  MeV ( $\Gamma = 2.6 \pm 0.4$  MeV,  $85 \pm 15\%$  EWSR), thus coinciding with the findings of the present work.

The excitation energy of the isoscalar E2 resonance ( $62 \text{ A}^{-1/3}$ ) is in good agreement with the calculations of Bohr and Mottelson ( $58 \text{ A}^{-1/3}$ ). Interpolation of the

calculations of Liu and Brown shows a possible E2 transition at 12.0 MeV, exhausting approximately 65% of the isoscalar EWSR. The possibly underlying E3 has been predicted by Bohr and Mottelson, but with a strength of only 2%. From Liu and Brown an isovector E3 with a strength of 14% can be expected in this region. Again, it is not possible to answer the question whether the model fails or whether the underlying transition really exists.

A second E2 transition (see Fig. 10) was found at  $E_x = 10.0 \pm 0.2$  MeV ( $52 A^{-1/3}$ ) with  $\Gamma = 1.8 \pm 0.2$  MeV, which exhausts  $6.5 \pm 1.5\%$  of the isovector and  $9.0 \pm 2.0\%$  of the isoscalar EWSR. The isoscalar character seems to be more likely due to the position of the resonance in the spectrum, although from Liu and Brown an isovector E2 with 13% strength can be expected in this region. An isoscalar E2 with 15% strength can be predicted at approximately 6 MeV from Liu and Brown. However, the line in question may as well be a monopole transition, since the form factors of the E0 and E2 transitions are basically the same. An E0 assignment would result in a strength of 13% of the EWSR (IS).

#### D. THE ISOVECTOR GIANT QUADRUPOLE RESONANCE

Figure 11 shows the experimental form factors of a resonance found at  $E_x = 25.0 \pm 0.6$  MeV ( $\Gamma = 6.5 \pm 0.5$  MeV) and an E2 GT form factor curve along with a mixed model form factor curve, having equal contributions from GT and

SJ transition densities. The mixed model was taken into consideration here since the resonance found is believed to be the isovector GQR. Myers et al. developed this model, which was described earlier in detail, for the GDR, which is an isovector transition. It can be seen from Figure 11 that the experimental results are in much better agreement with the mixed model than with the GT model. The resonance exhausts  $41 \pm 8\%$  of the isovector EWSR in the mixed model and  $77 \pm 25\%$  in the GT model.

It was also considered that higher multipolarities might be lying under this E2 transition. By fitting the GT curve to the lower limit of the form factor from the 80 MeV/90° experiment, the difference between the curve and the results was taken and plotted versus  $q$  (see Fig. 12). From this graph an E3 or E4, or a mixture of both, under this E2 is a distinct possibility. In this case the GQR exhausts roughly 55% of the isovector EWSR. The possible E3 beneath dissipates 23% of the isoscalar and 16% of the isovector octupole strength. One can expect a 14% strong isovector E3 from Liu and Brown in this region.

The experimental form factor representing the 80 MeV/90° experiment in Figure 11 ( $E_x = 25$  MeV) demands some comment, in particular some explanation of the behavior of the line found at  $E_x = 30.5$  MeV. This resonance, which will be described later in more detail, was found in the 92 MeV/90° and 92 MeV/105° experiments, but not in the 80 MeV/90°

spectrum. Since the statistics of the data generally worsen at higher excitation energy due to the constant dispersion of the magnetic spectrometer, it was assumed that the resonance at  $E_x = 30.5$  MeV might also be present in the low q experiment, but that it could not be seen due to the poor statistics. Thus the area the resonance should have in the 80 MeV/90° experiment was calculated from the high q results and the line was fitted into the 80 MeV/90° spectrum by "freezing" its parameters. This had a remarkable influence on the neighboring resonances, as anticipated. It was in particular the form factor of the isovector GQR which increased by some 50%, thus allowing a much better fit of an E2 form factor curve and making the E2 assignment for the resonance in question consistent with investigations of other nuclei, namely:  $^{58}\text{Ni}$  (BeaK 77),  $^{89}\text{Y}$  (PitB 77),  $^{90}\text{Zr}$  (FukT 76),  $^{142}\text{Nd}$  (Sch 76),  $^{165}\text{Ho}$  (MooB 76),  $^{181}\text{Ta}$  (HicA 77),  $^{197}\text{Au}$  (PitB 74),  $^{208}\text{Pb}$  (PitB 74), and  $^{238}\text{U}$  (HouM 77). There can thus be little doubt that the resonance found is the isovector E2 transition. It is in agreement with the predictions of Bohr and Mottelson and also Liu and Brown, from whose calculations a possibly split ( $\Delta T = 1$ ) resonance with 65% EWSR can be expected in this region. An effort on our part to fit a split resonance, as Richter (Ric 77) seems to have seen in  $^{144}\text{Sm}$ , was not successful.

## E. THE GIANT OCTUPOLE RESONANCES

### 1. General

From shell model calculations there are four predicted E3 transitions (Ham 72) at  $25 \text{ A}^{-1/3}$  and  $106 \text{ A}^{-1/3} \text{ MeV}$  (isoscalar), and at  $53 \text{ A}^{-1/3}$  and  $195 \text{ A}^{-1/3} \text{ MeV}$  (isovector). For  $^{140}\text{Ce}$  these resonances in terms of energy become 4.8, 20.4, 10.2, and 37.6 MeV respectively. Three of these could be located with little doubt in this work. The  $53 \text{ A}^{-1/3} \text{ MeV}$  transition is expected to be very weak and is probably hidden under stronger resonances in this area of the spectrum, corresponding to the E3 transition which possibly exists under the isoscalar GQR ( $E_x = 12 \text{ MeV}$ ), as discussed earlier.

### 2. The Isoscalar Giant Octupole Resonances

The low lying isoscalar E3 transition is thought to be the resonance found at  $E_x = 6.0 \pm 0.2 \text{ MeV}$  ( $31 \text{ A}^{-1/3}$ ) with  $\Gamma = 1.7 \pm 0.2 \text{ MeV}$  (see Fig. 10), exhausting  $19 \pm 3\%$  of the isoscalar EWSR. This is in very good agreement with the calculations of Bohr and Mottelson (BohM 75) and Hamamoto (Ham 72). It also agrees with Liu and Brown (LiuB 76), who allow one to expect an isoscalar E3 at 6 MeV, dissipating 18% of the isoscalar EWSR. Moss et al. (MosY 76) observed a giant resonance at  $E_x \sim 32 \text{ A}^{-1/3} \text{ MeV}$  in  $(\alpha, \alpha')$  spectra in nuclei from  $^{90}\text{Zr}$  to  $^{154}\text{Sm}$  and reported it to be an E3 state. The EWSR fraction ranged from 16 to 22% in that experiment. Figure 10 shows that other transitions can be

ruled out; however, some caution should be used since the region in which this resonance was found might be distorted by the "ghost peak", as previously described.

The line found at  $E_x = 22.0 \pm 0.6$  MeV with  $\Gamma = 4.8 \pm 0.3$  MeV (see Fig. 11) was identified with the high lying ( $3\hbar\omega_0$ ) isoscalar GOR. It exhausts  $19 \pm 2\%$  of the EWSR. Other states (E2 and E4) cannot be ruled out completely since the statistical errors for this resonance are fairly large. The E3 character, though, is in good agreement with Bohr and Mottelson, Hamamoto and Liu and Brown. Liu and Brown calculate an E3 ( $\Delta T = 0$ ) transition which is to be expected around 22 MeV, with a strength of roughly 40%. This strength may be partly under the 25 MeV resonance.

### 3. The Isovector Giant Octupole Resonance

It was mentioned before that the low lying isovector E3 transition could not be identified explicitly in the spectra investigated.

The identity of the broad resonance found at  $E_x = 37.5 \pm 1.0$  MeV was determined to be the  $3\hbar\omega_0$  isovector octupole transition. An E0, probably of isovector character, cannot be ruled out, as will be explained later. Assuming the transition to be an E3, it dissipates  $75 \pm 10\%$  of the isovector EWSR. Assuming an E0 ( $\Delta T = 1$ ), it has a strength of roughly 130%. Naturally, a mixture of E0 and E3 states would also be possible.

The error flags in Figure 11 deserve some explanation. The 92 MeV/90° and the first run of the 92 MeV/105° experiment (it was run twice to ensure correctness of the

data) showed scatter outside the statistics beyond  $E_x = 43$  MeV. It was therefore first attempted to fit the 92 MeV/90° and the combined 92 MeV/105° spectra from 4 to only 43 MeV excitation energy. Doing so, the form factors of the resonance in question was compatible with both E0 and E3 transitions. Since it is known from experience that one should always attempt to measure and fit a spectrum at least one to two half widths beyond the excitation energy of the resonance in question, it was decided to fit the 92 MeV/90° and only the second 92 MeV/105° spectrum to full range (48 MeV). The results of these spectra were then taken for the resonance at  $E_x = 37.5$  MeV. Figure 11 shows only the results of the latter fit, while Figure 3 corresponds to the first one.

The assignment of an E3 transition to this resonance is in excellent agreement with Bohr and Mottelson and Hamamoto ( $195 \text{ A}^{-1/3}$ ), however their prediction of 97% strength is higher than what was found in this work. From Liu and Brown an E3 ( $\Delta T = 1$ ) can be expected at  $E_x = 35 \pm 6$  MeV, exhausting 65% of the EWSR. They also calculate an E0 ( $\Delta T = 1$ ) state in the region between 28 and 40 MeV, with 60% strength.

The  $195 \text{ A}^{-1/3}$  MeV resonance has been observed before in  $^{165}\text{Ho}$  (MooB 76),  $^{181}\text{Ta}$  (HicA 77),  $^{197}\text{Au}$  (PitB 74),  $^{208}\text{Pb}$  (PitB 74),  $^{238}\text{U}$  (HouM 77), and has been identified as a possible isovector octupole or monopole state in these nuclei.

## F. OTHER RESONANCES

Three other resonances were found. The first was at  $E_x = 7.4 \pm 0.2$  MeV ( $38 A^{-1/3}$ ) with  $\Gamma = 1.45 \pm 0.2$  MeV (see Fig. 10). It was not possible to determine whether this resonance is an E3, E4 or a state of even higher multipolarity. Considering it to be an E4 transition, it exhausts some 5% of the isoscalar EWSR. As an E3 state, on the other hand, it represents only 4% of the isoscalar strength. An explanation as to why it was difficult to determine the multipolarity is that the "ghost peak" lies in the general vicinity of this resonance and affects the ability to fit this line properly into the spectra.

At  $E_x = 8.6 \pm 0.2$  MeV a peak was found which had previously been seen by Pitthan (Pit 73) and had been identified as a magnetic dipole, M1. Since the scattering angles used in our experiments do not favor the evaluation of magnetic transitions, no effort was made to investigate this resonance.

Finally a line was found at  $E_x = 30.5 \pm 1.0$  MeV ( $158 A^{-1/3}$ ) with  $\Gamma = 6.7 \pm 0.8$  MeV (see Fig. 11). It could not be determined whether it is an E3 or E4 transition or a mixture of both. As a hexadecapole transition it would exhaust  $86 \pm 23\%$  of the isoscalar EWSR, as an E3 state it would dissipate  $38 \pm 4\%$  and  $27 \pm 3\%$  of the isoscalar and isovector strength respectively. Hamamoto (Ham 72) predicts an E4 ( $\Delta T = 0$ ) state at approximately  $E_x = 29$  MeV

(49% EWSR) and from Liu and Brown an isoscalar E4, exhausting 40% of the EWSR can be expected in the region between 19 and 40 MeV. It, therefore, seems possible that the peak found is really a mixture of octupole and hexadecapole transitions. The octupole state might be the same which contributes to the rise of the isovector GQR at  $E_x = 25$  MeV for high momentum transfer compared to the GT model.

## VI. CONCLUSIONS

The resonances at excitation energies of  $52 \text{ A}^{-1/3} \text{ MeV}$  (E2, 9% EWSR),  $62 \text{ A}^{-1/3} \text{ MeV}$  (E2, 63% EWSR) and  $80 \text{ A}^{-1/3} \text{ MeV}$  (E1, 122% EWSR in the mixed model of Myers et al.) found by Pitthan (Pit 73), were verified in this work. In addition new resonances were found at excitation energies of  $31 \text{ A}^{-1/3} \text{ MeV}$  (E3, 19% EWSR),  $38 \text{ A}^{-1/3} \text{ MeV}$  (E3 or E4, 5% EWSR),  $114 \text{ A}^{-1/3} \text{ MeV}$  (E3, 19% EWSR),  $130 \text{ A}^{-1/3} \text{ MeV}$  (E2, 41% EWSR in the mixed model),  $158 \text{ A}^{-1/3} \text{ MeV}$  (E3 or E4, 38 or 86% EWSR) and  $195 \text{ A}^{-1/3} \text{ MeV}$  (E3, 75% EWSR). For all but two of the transitions that were detected, determination of the multipolarity could be made with little doubt. Further investigation of the resonances with excitation energies of  $38 \text{ A}^{-1/3}$  and  $158 \text{ A}^{-1/3} \text{ MeV}$ , however, is necessary.

In several cases it was impossible to determine whether the models used were incorrect or whether there were other states beneath the resonances being investigated. These cases include the GDR, where our results suggested that either the newly developed model by Myers et al. (MyeS 77) is right or that an E0 state exists under the E1. They include further both the isoscalar and isovector GQR. In the isoscalar case it could not be determined whether the half density radius  $c_{tr} = 0.95 c$  is correct in the Fermi charge distribution for the excited state, or whether a higher multipolarity underlies this transition. In the

isovector case our results fitted the mixed model (GT + SJ) form factor curve better than a GT curve and it could not be decided whether the model proposed by Myers et al. is also applicable for higher multipolarities than E1, or whether an E3 or E4 state exists under the line in question.

In all three spectra the region between 27 and 48 MeV excitation energy must be treated with caution. Due to the constant dispersion of the magnetic spectrometer, the statistics are poorer in this region compared to the region of lower excitation energy. It was further realized that it is very difficult to determine half widths and excitation energies of resonances believed to exist in 27 to 48 MeV region since individual peaks almost never appear in this part of the raw spectra.

Finally, the comparison of our results with the calculations of Liu and Brown (LiuB 76) deserves some comment. It must again be emphasized that the "predictions" of Liu and Brown that were referred to were based on the interpolation of their calculations for  $^{208}\text{Pb}$  and  $^{90}\text{Zr}$ . The agreement between these "predictions" and the findings of this work, however, are quite remarkable and suggests that actual calculations on this basis should be made for  $^{140}\text{Ce}$ .

TABLE I. CALCULATIONS FROM LIU AND BROWN FOR  $^{140}\text{Ce}$ .\*

$\lambda$	T	% Strength	$E_x$ (MeV)
0	0	34	19.0
0	0	55	21.0 - 27.0
0	1	9	11.0 - 21.0
0	1	15	21.0 - 27.5
0	1	50	27.5 - 37.0
0	1	15	37.0 - 49.0
1	1	43	15.0
1	1	36	18.0
1	1	15	23.0 - 35.0
2	0	15	6.0
2	0	65	12.0
2	0	10	17.0 - 27.0
2	1	13	0.0 - 23.0
2	1	35	24.0 - 26.0
2	1	29	28.0
2	1	20	32.0 - 50.0
3	0	18	6.0
3	0	7	10.0
3	0	12	12.0 - 18.0
3	0	39	22.0
3	0	13	28.0 - 37.0
3	1	3	0.0 - 13.0
3	1	14	13.0 - 28.0
3	1	65	28.0 - 43.0
3	1	15	43.0 - 60.0
4	0	26	0.0 - 18.0
4	0	40	18.0 - 40.0
4	0	?	40.0
4	1	17	0.0 - 30.0
4	1	69	30.0 - 70.0

\* The calculations are interpolations of the results for  $^{90}\text{Zr}$  and  $^{208}\text{Pb}$  of Liu and Brown (LiuB 76)

TABLE II. EXPERIMENTAL PARAMETERS

Spectrometer Angle (Deg)	Machine Energy (MeV)	Elastic Energy (MeV)	Elastic Peak Halfwidth (MeV)	Elastic Area (counts/ $\mu$ coul)
90	79.57	79.41	0.447	2551.3
90	92.15	91.98	0.529	1238.6
105	92.83	92.62	0.519	1110.0
Spectrometer Energy Range (MeV) Elastic      Inelastic		Bremsstrahlung Correction (%)	Schwinger Correction (%)	
82.5 - 74.5	77.0 - 27.0	16.63	17.00	
95.0 - 85.5	88.0 - 40.0	16.54	17.42	
95.0 - 85.5	88.0 - 40.0	19.59	18.02	
Elastic Recoil		Effective Target Thickness ( $\text{gm}/\text{cm}^2$ )	Elastic Momentum Transfer ( $\text{fm}^{-1}$ )	
1.0006084		0.1782	0.57	
1.0007048		0.1782	0.66	
1.0008926		0.2070	0.75	

Target thickness for all three experiments:  $126 \text{ mg}/\text{cm}^2$

TABLE III. DATA ANALYSIS RESULTS

## 80 MeV/90 Degrees

Energy (MeV)	$q$ (fm $^{-1}$ )	Multipolarity (E $\lambda$ )	Form Factor Squared	B Value (fm $^2\lambda$ )
6.0	0.549	3	$2.87 \times 10^{-4}$	$1.24 \times 10^5$
7.4	0.544	3, 4 (?)	$4.53 \times 10^{-5}$	$3.56 \times 10^6$
10.0	0.536	2	$1.09 \times 10^{-4}$	$5.88 \times 10^2$
12.2	0.528	2	$4.75 \times 10^{-4}$	$1.94 \times 10^3$
15.3	0.518	1	$5.51 \times 10^{-4}$	$3.51 \times 10^1$
22.0	0.498	3	$6.90 \times 10^{-5}$	$3.25 \times 10^4$
25.0	0.489	2	$3.19 \times 10^{-4}$	$9.38 \times 10^2$
38.0	0.455	3	$2.45 \times 10^{-4}$	$1.30 \times 10^5$

## 92 MeV/90 Degrees

6.0	0.639	3	$3.06 \times 10^{-4}$	$1.30 \times 10^5$
7.4	0.634	3, 4 (?)	$5.53 \times 10^{-5}$	$2.60 \times 10^6$
10.0	0.626	2	$4.88 \times 10^{-4}$	$4.38 \times 10^2$
12.0	0.619	2	$3.54 \times 10^{-4}$	$2.13 \times 10^3$
15.4	0.608	1	$3.50 \times 10^{-4}$	$4.56 \times 10^1$
22.0	0.587	3	$9.28 \times 10^{-5}$	$3.71 \times 10^4$
25.0	0.578	2	$3.57 \times 10^{-4}$	$1.23 \times 10^3$
30.0	0.563	3, 4 (?)	$1.61 \times 10^{-4}$	$1.02 \times 10^7$
37.5	0.543	3	$3.15 \times 10^{-4}$	$1.21 \times 10^5$

## 92 MeV/105 Degrees

6.0	0.722	3	$2.69 \times 10^{-4}$	$1.48 \times 10^5$
7.4	0.717	3, 4 (?)	$5.29 \times 10^{-5}$	$2.29 \times 10^6$
10.0	0.707	2	$1.83 \times 10^{-4}$	$3.84 \times 10^3$
12.0	0.699	2	$1.66 \times 10^{-4}$	$1.96 \times 10^3$
15.4	0.686	1	$1.82 \times 10^{-4}$	$4.17 \times 10^1$
22.0	0.661	3	$9.42 \times 10^{-5}$	$4.06 \times 10^4$
25.0	0.650	2	$2.45 \times 10^{-4}$	$1.14 \times 10^6$
31.5	0.627	3, 4 (?)	$1.62 \times 10^{-4}$	$7.30 \times 10^5$
38.0	0.607	3	$3.24 \times 10^{-4}$	$1.16 \times 10^0$

(1) Based on the assumption that it is an E4

(2) Using  $c_{tr} = 0.95 c$ (3) Using the Myers-Swiatecki model with  $\alpha = 0.76$ (4) Using the Myers-Swiatecki model with  $\alpha = 1.00$

TABLE IV. GIANT RESONANCES

$E_X$ (MeV)	$E_X A^{-1/3}$	$\Gamma$ (MeV)	$E\lambda$	$\Delta T$	$B_{\text{exp}}(\text{fm}^{2\lambda})$ [1]	$\Gamma_\gamma^0$ (eV)	$R^{[2]}$	Std. [3] Dev.	Total [4] Error
6.0±0.2	31	1.7±0.2	3	0	1.34x10 <sup>5</sup>	2.02x10 <sup>-3</sup>	19	±3	±6
10.0±0.2	52	1.8±0.2	2	0	4.30x10 <sup>2</sup>	7.59x10 <sup>0</sup>	9	±2	±4
			0	0	7.70x10 <sup>2</sup>	1.03x10 <sup>3</sup>	13	±2	±6
12.0±0.2	62	2.8±0.2	2	0	2.48x10 <sup>3</sup>	9.98x10 <sup>1</sup>	63	±17	±13
			2	0	2.01x10 <sup>3</sup>	8.07x10 <sup>1</sup>	50	±5	[5] ±10 [6]
15.3±0.2	79	4.4±0.2	1	1	4.08x10 <sup>1</sup>	5.10x10 <sup>4</sup>	122	±12	±20
			1	1	5.51x10 <sup>1</sup>	6.89x10 <sup>4</sup>	167	±40	±27 [8]
22.0±0.6	114	4.8±0.3	3	0	3.67x10 <sup>4</sup>	4.92x10 <sup>0</sup>	19	±2	±10
25.0±0.6	130	6.5±0.5	2	1	1.10x10 <sup>3</sup>	1.73x10 <sup>3</sup>	41	±8	±15 [9] ±28 [10]
			2	1	2.06x10 <sup>3</sup>	3.25x10 <sup>3</sup>	77	±25	
37.5±1.0	195	8.5±1.0	3	1	1.22 10 <sup>5</sup>	6.84x10 <sup>2</sup>	75	±10	±25

TABLE VI. GIANT RESONANCES (Continued)

NOTES:

- [1] For the monopole the measured quantity is  $|M_{if}|^2$  (fm<sup>4</sup>)
- [2]  $R = E_x B(E\lambda) / \text{EWSR}(E\lambda, \Delta T) \times 100$
- [3] The error given is the standard deviation of the average sum rule exhaustion and is, therefore, more a measure for the fit to a certain model than a measure for the total uncertainty.
- [4] The total error is based on the maximum and minimum values found for the areas under the curves during the fitting procedure.
- [5] Using  $c_{tr} = 1.0c$ .
- [6] Using  $c_{tr} = 0.95c$ .
- [7] Using the Myers-Swiatecki (MS) model with  $\alpha = 0.76$ .
- [8] Using the Goldhaber-Teller model.
- [9] Using the Myers-Swiatecki (MS) model with  $\alpha = 1.0$ .
- [10] Using the Goldhaber-Teller model.

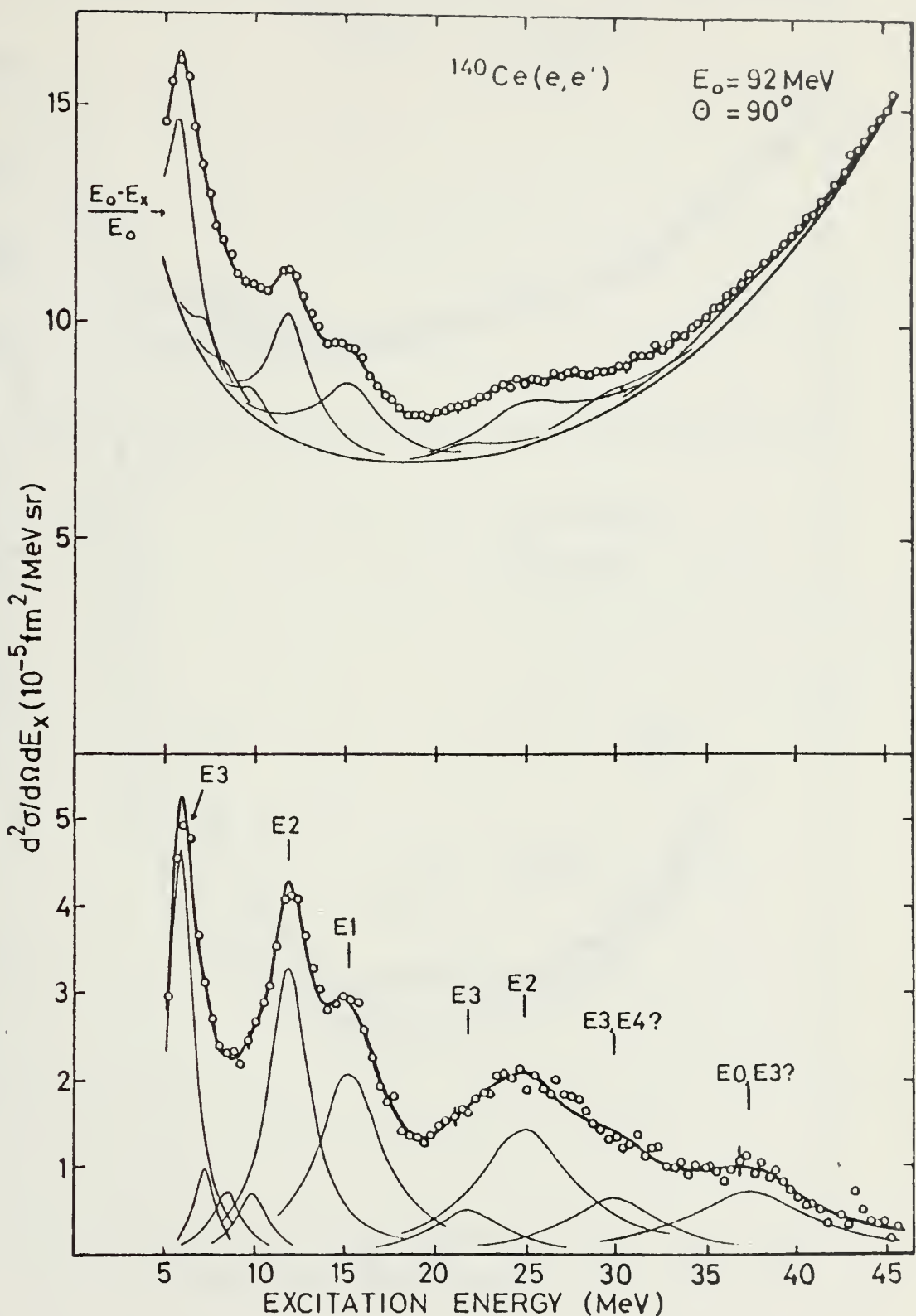


FIGURE 1. Inelastic  $^{140}\text{Ce}$  spectrum with and without background.

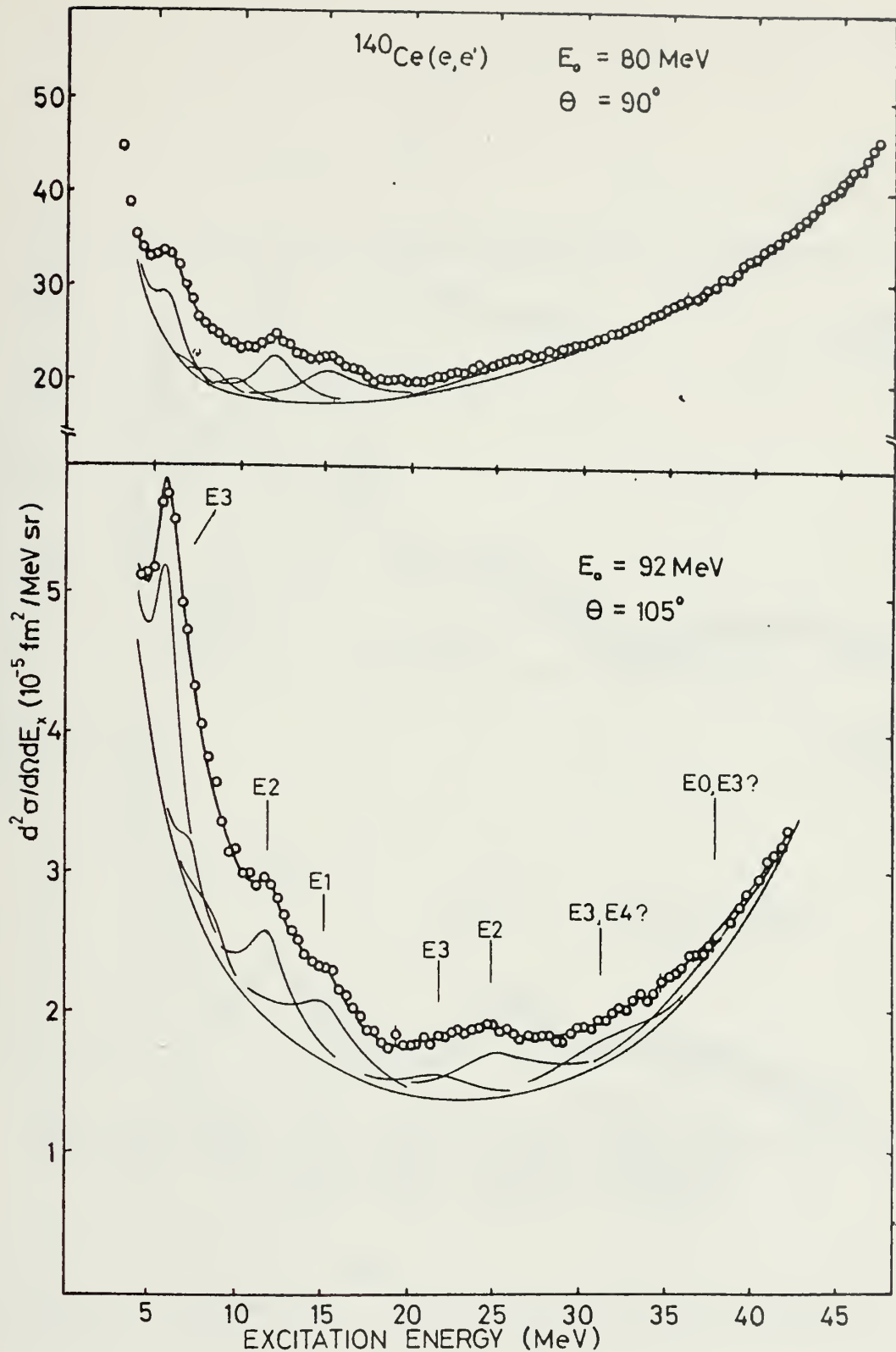


FIGURE 2. Inelastic  $^{140}\text{Ce}$  spectra with background.

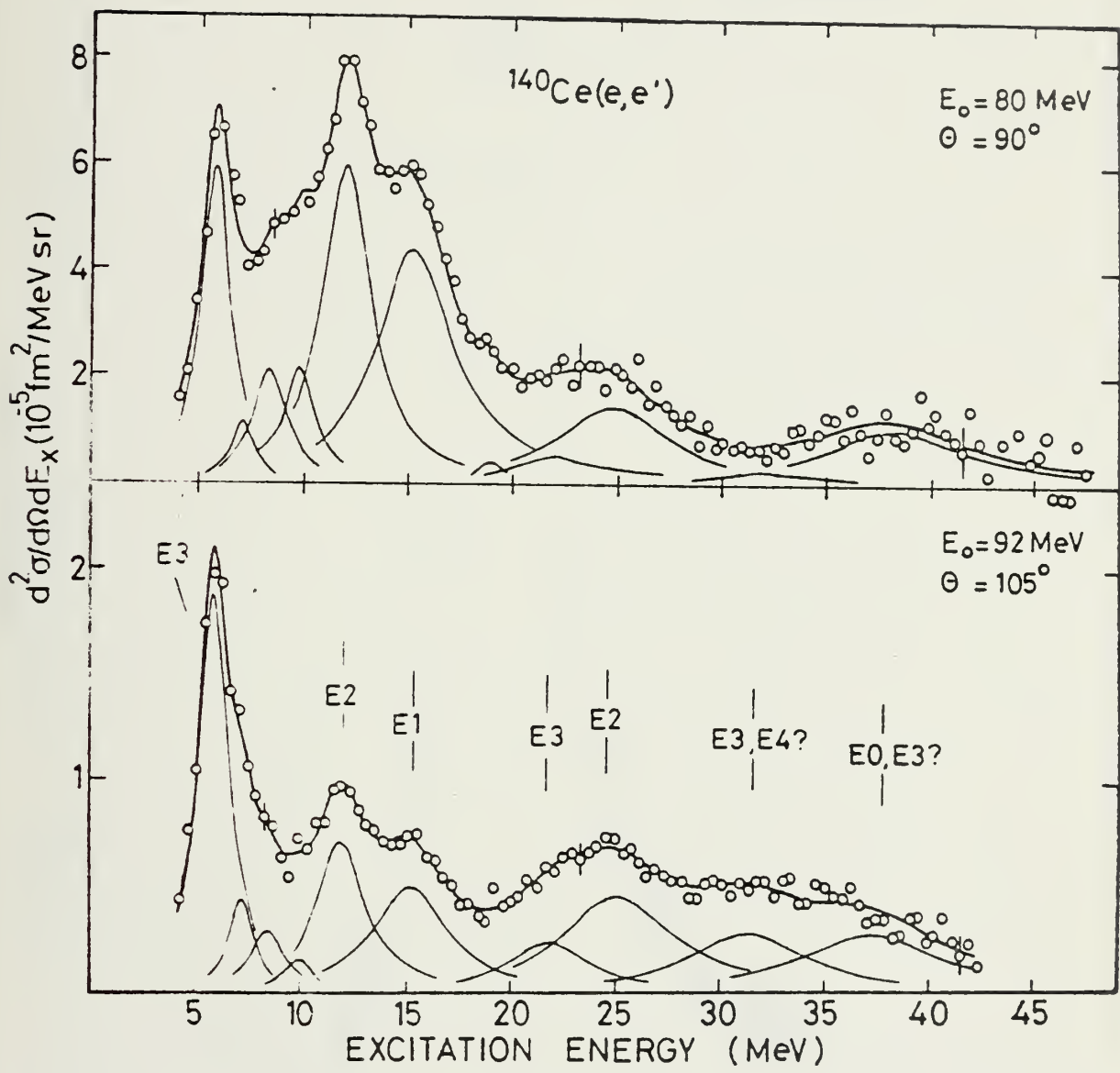


FIGURE 3. Inelastic  $^{140}\text{Ce}$  spectra without background.

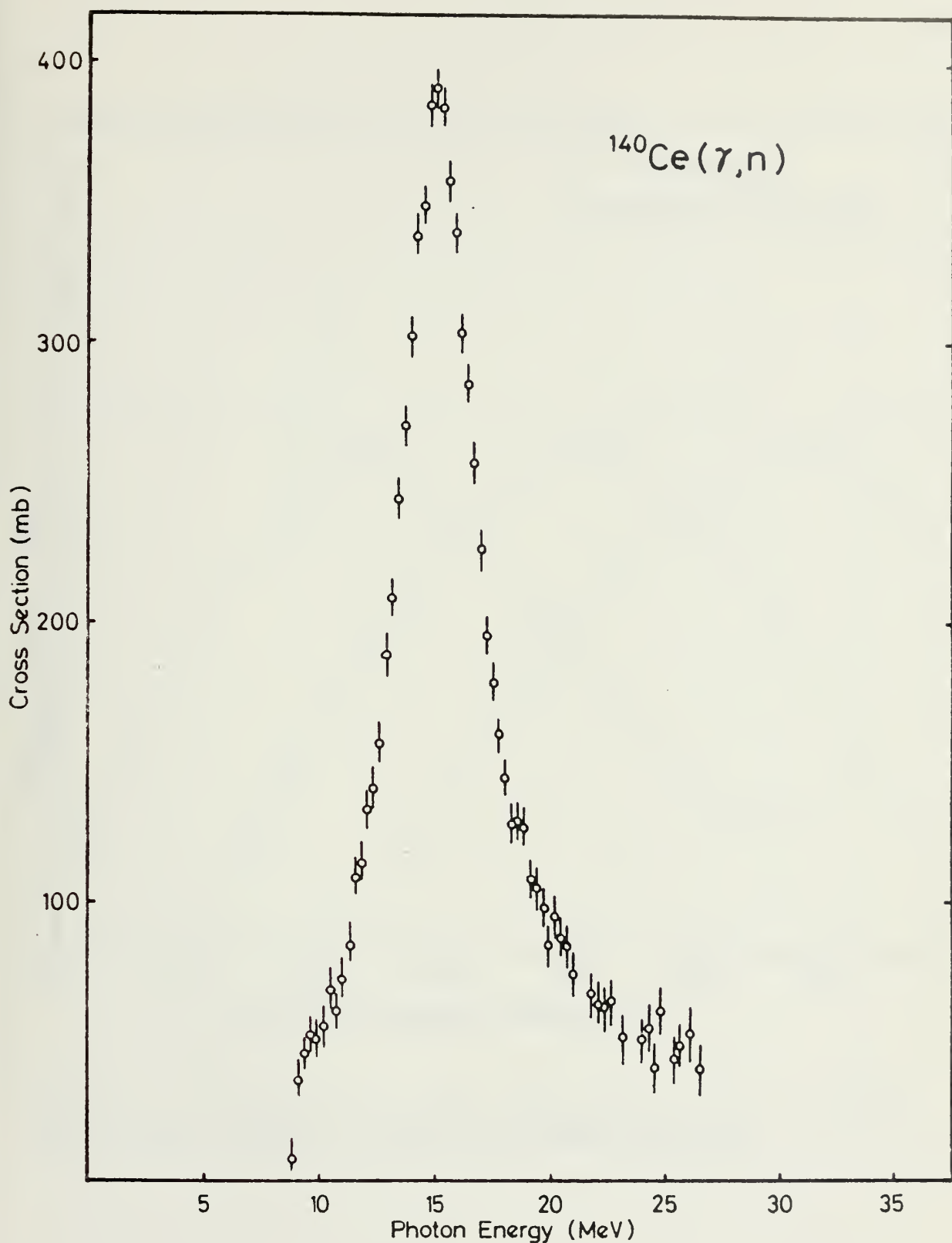


FIGURE 4. Photon absorption cross section of  $^{140}\text{Ce}$ .

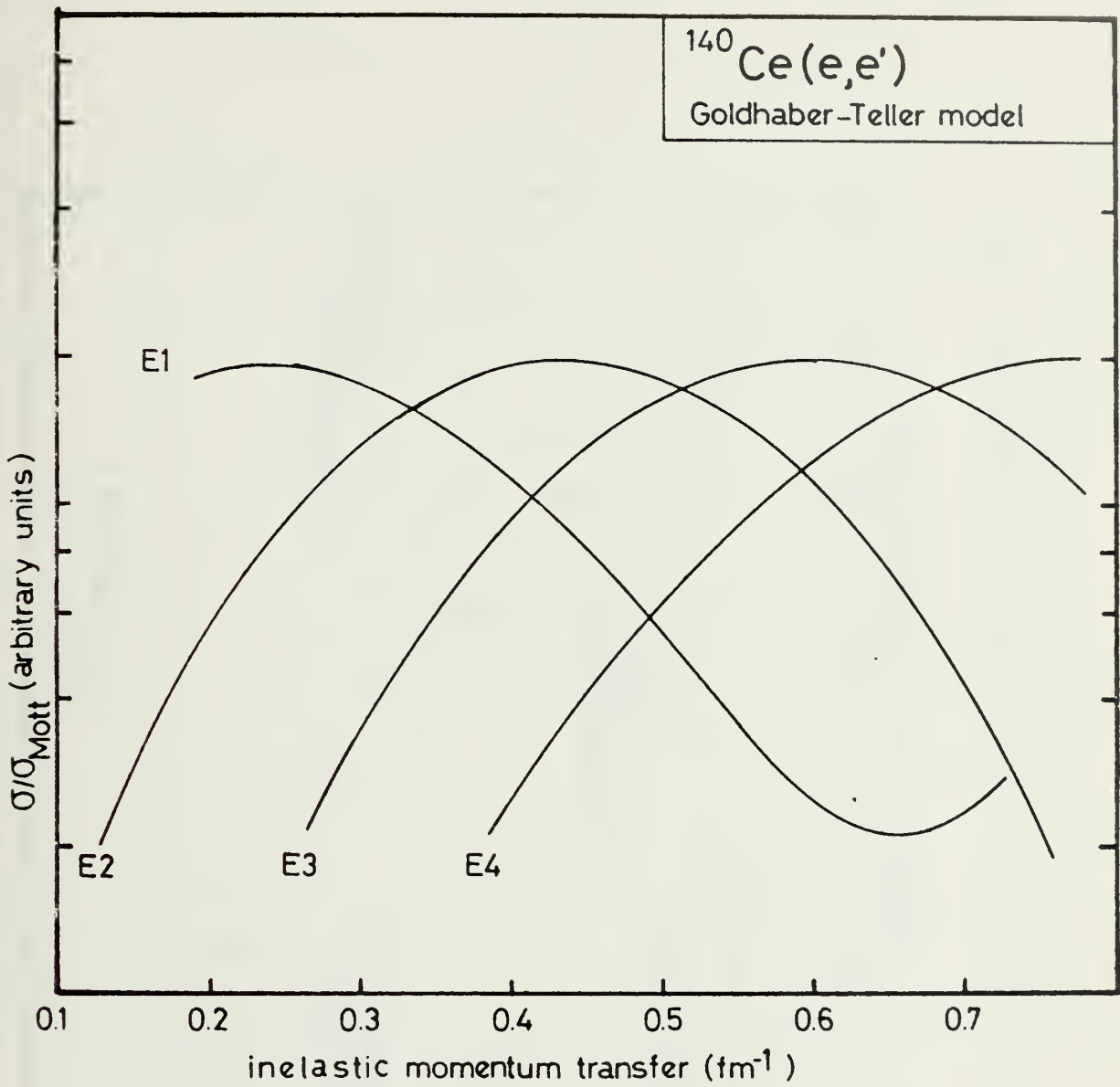


FIGURE 5. Comparison of DWBA cross sections for E1 to E4 transitions divided by the Mott cross sections.

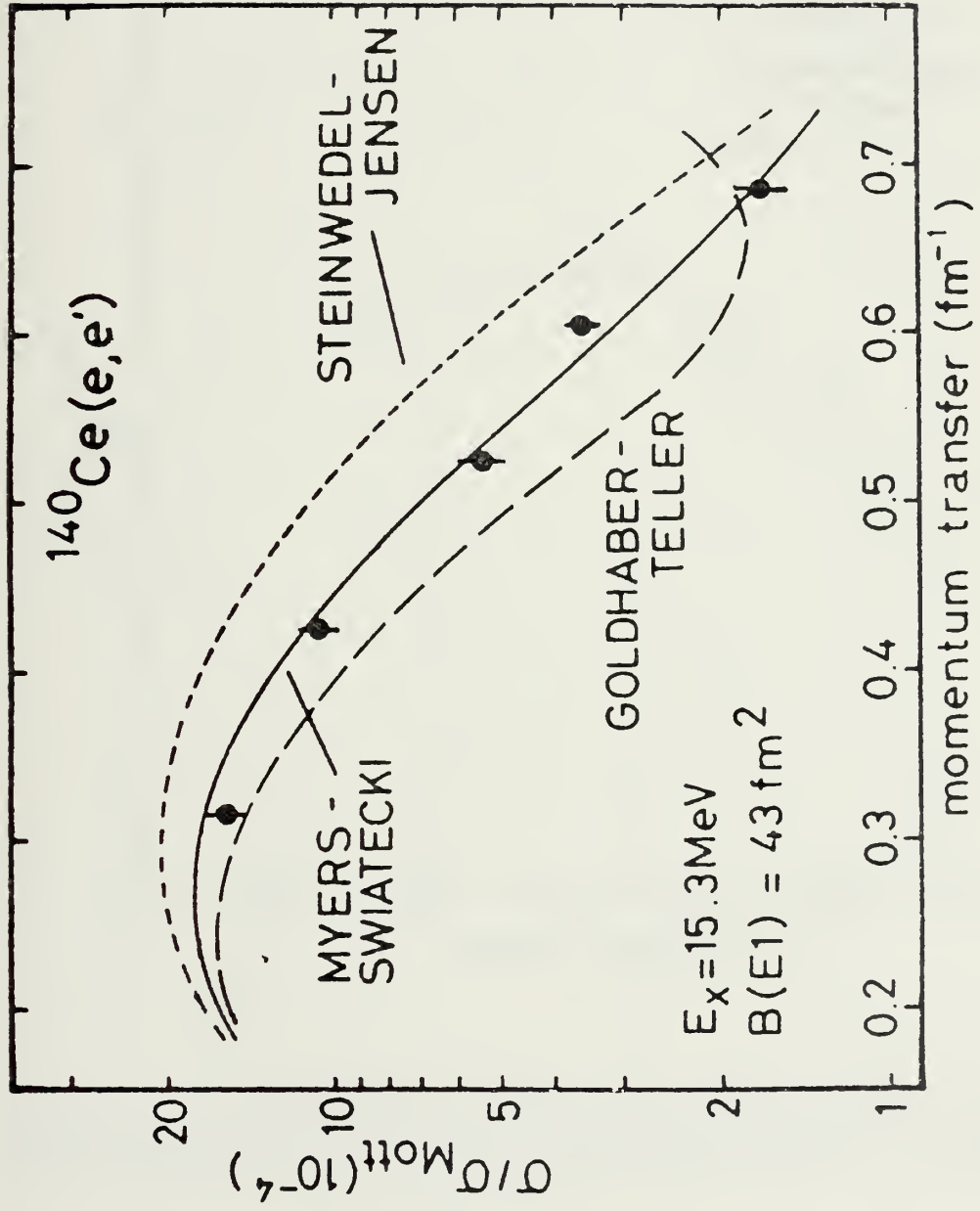


FIGURE 6. Comparison of the DWBA and experimental form factors for the resonance found at 15.3 MeV.

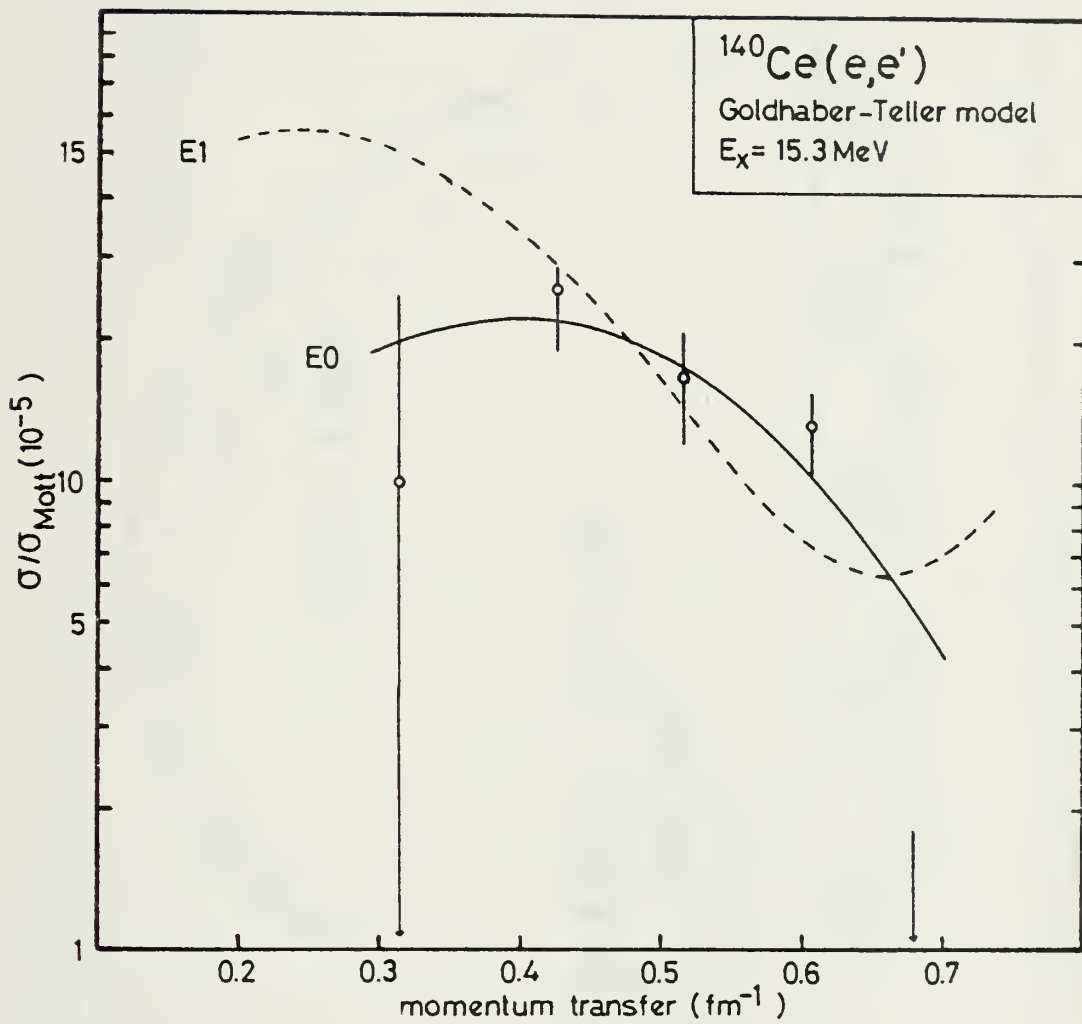


FIGURE 7. Comparison of the difference between the experimental form factor and the Goldhaber-Teller model and the DWBA form factors for the resonance found at 15.3 MeV.

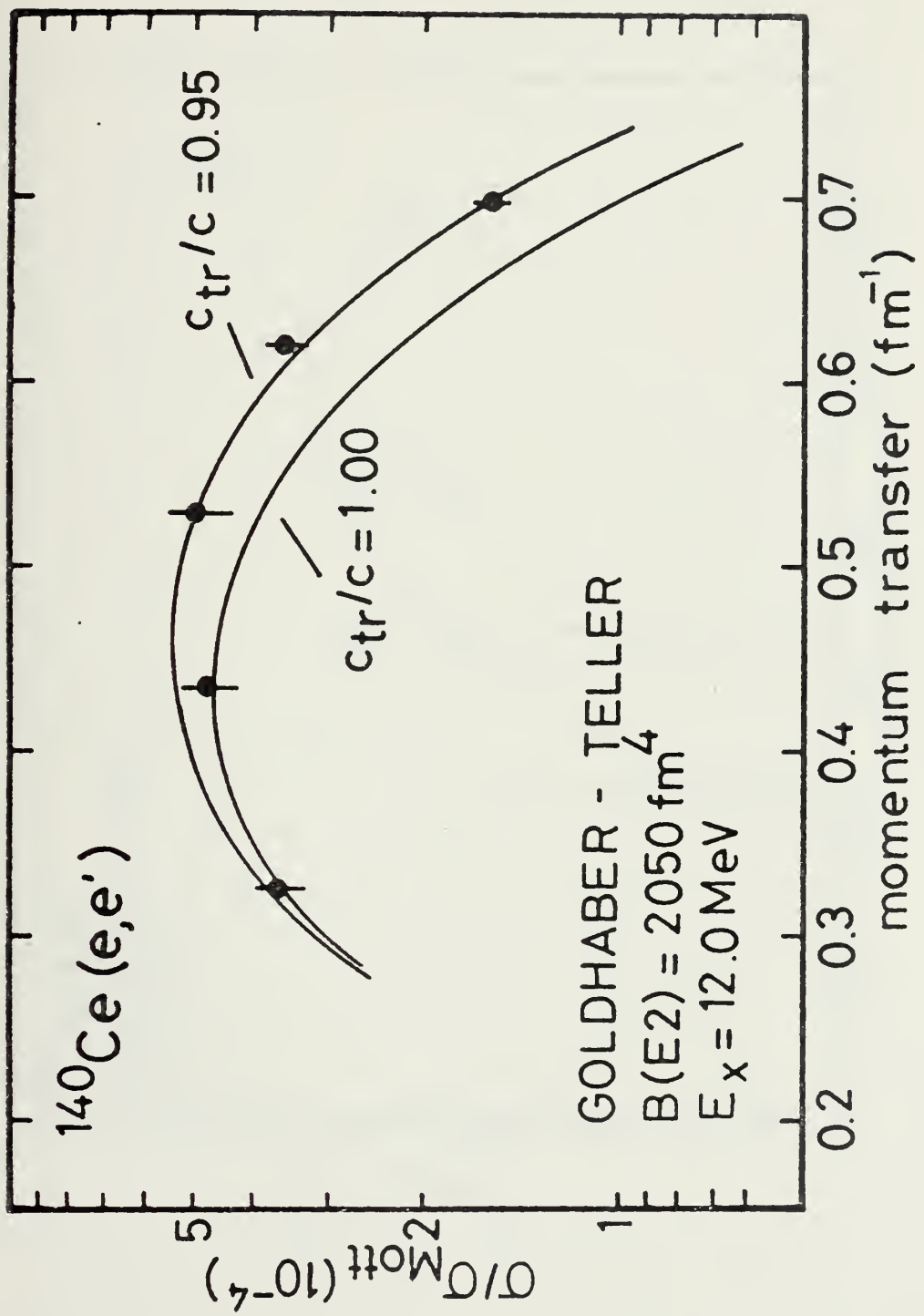


FIGURE 8. Comparison of the DWBA and experimental form factors for the resonance found at 12.0 MeV.

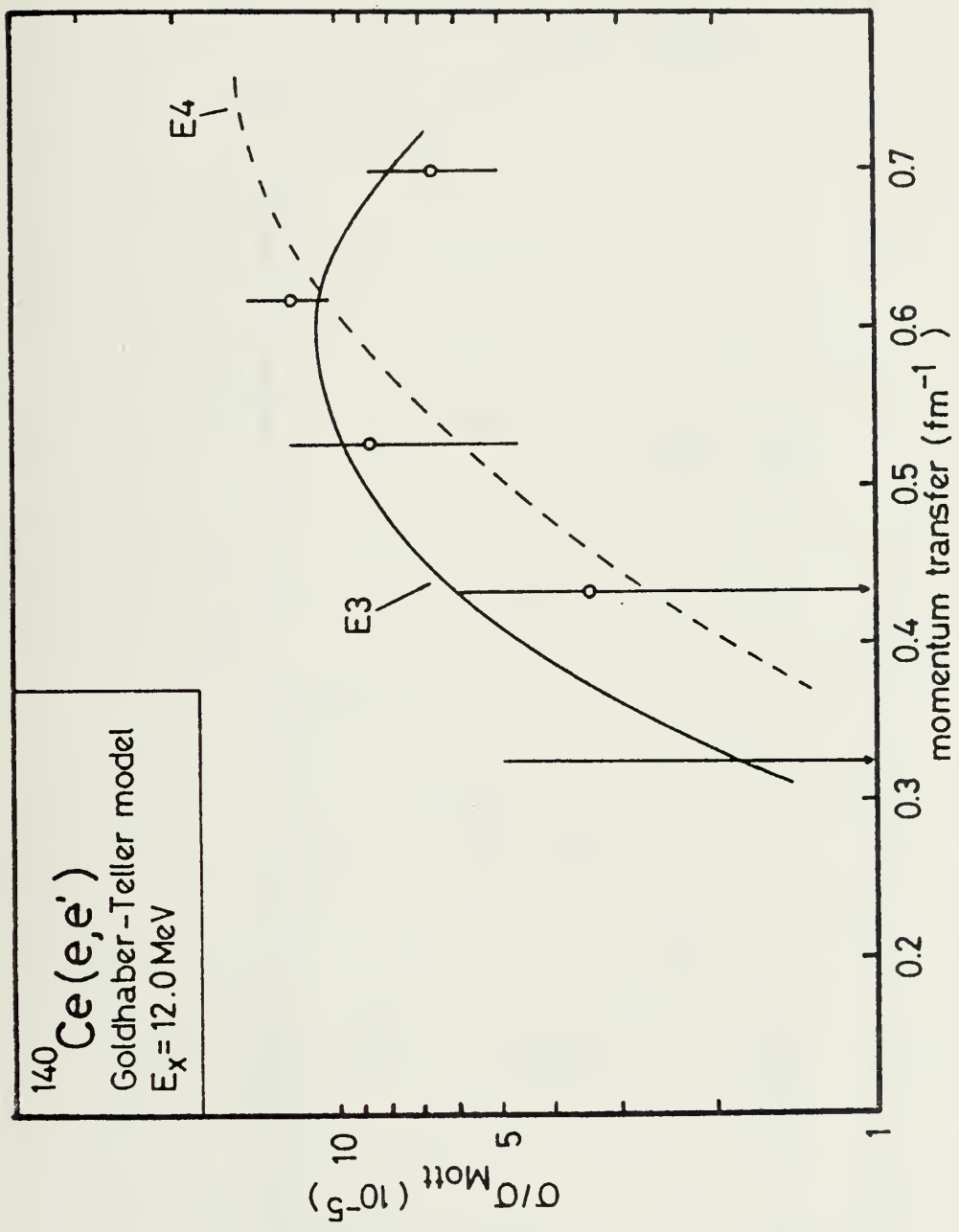


FIGURE 9. Comparison of the difference between the experimental and the DWBA form factors for the resonance found at 12.0 MeV.

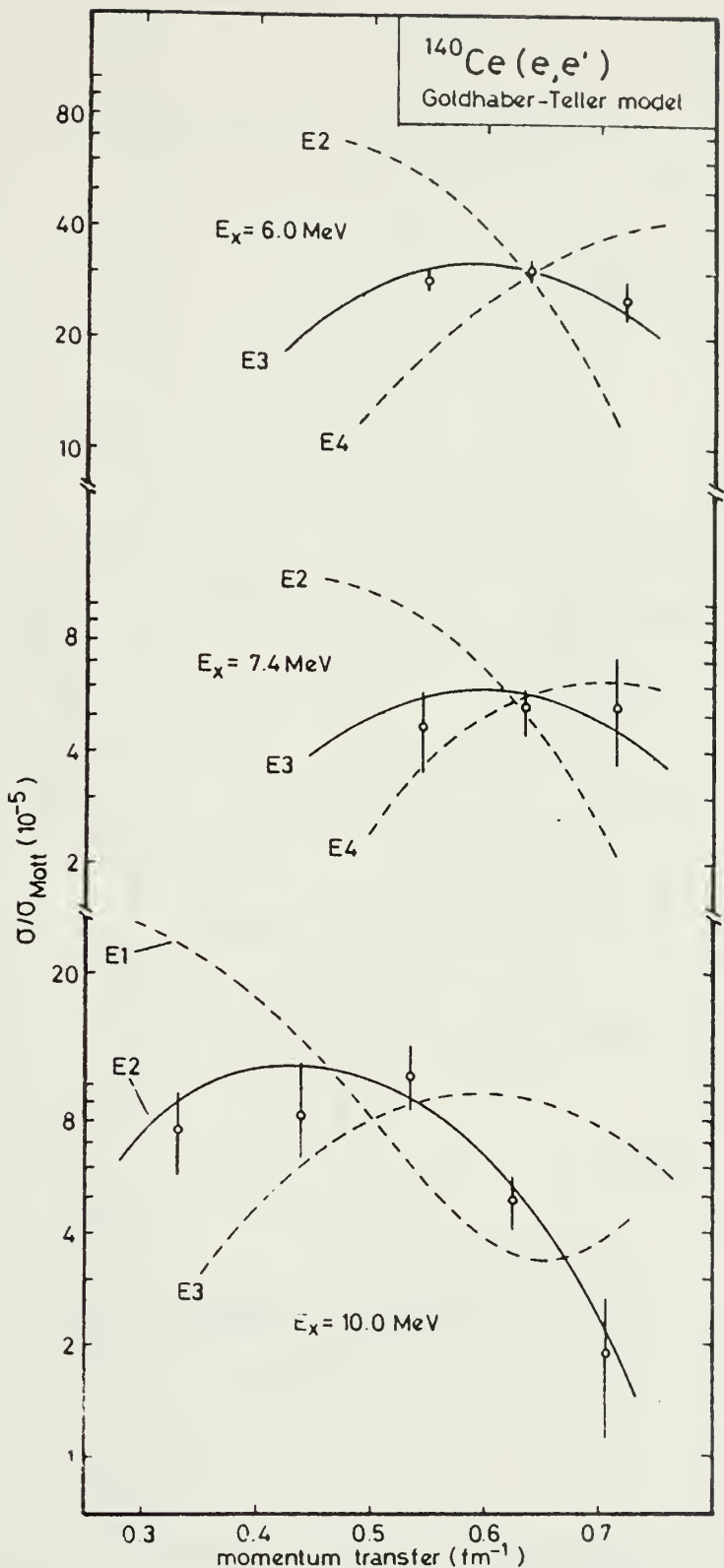


FIGURE 10. Comparison of the DWBA and experimental form factors for the resonances found at 6.0, 7.4, and 10.0 MeV.

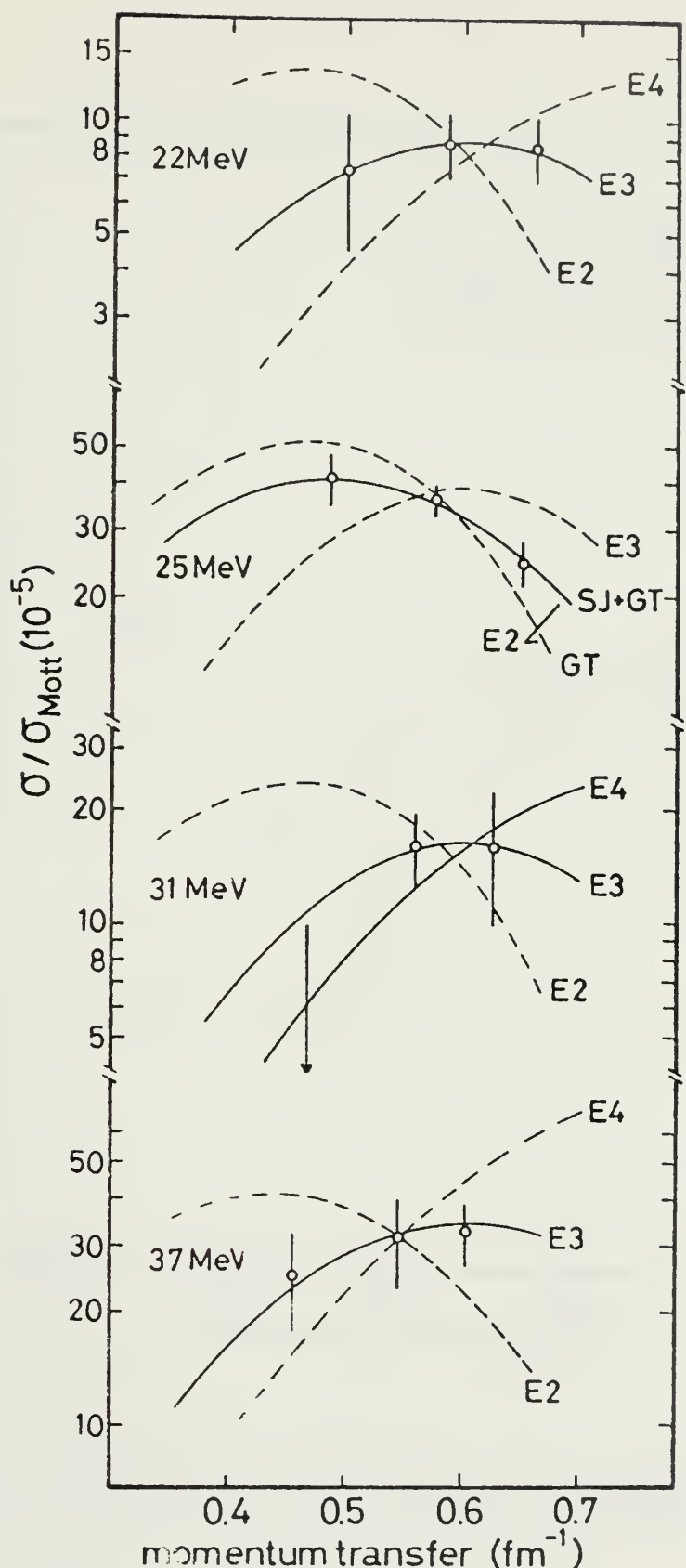


FIGURE 11. Comparison of the DWBA and experimental form factors for the resonances found at 22.0, 25.0, 31.0 and 37.5 MeV.

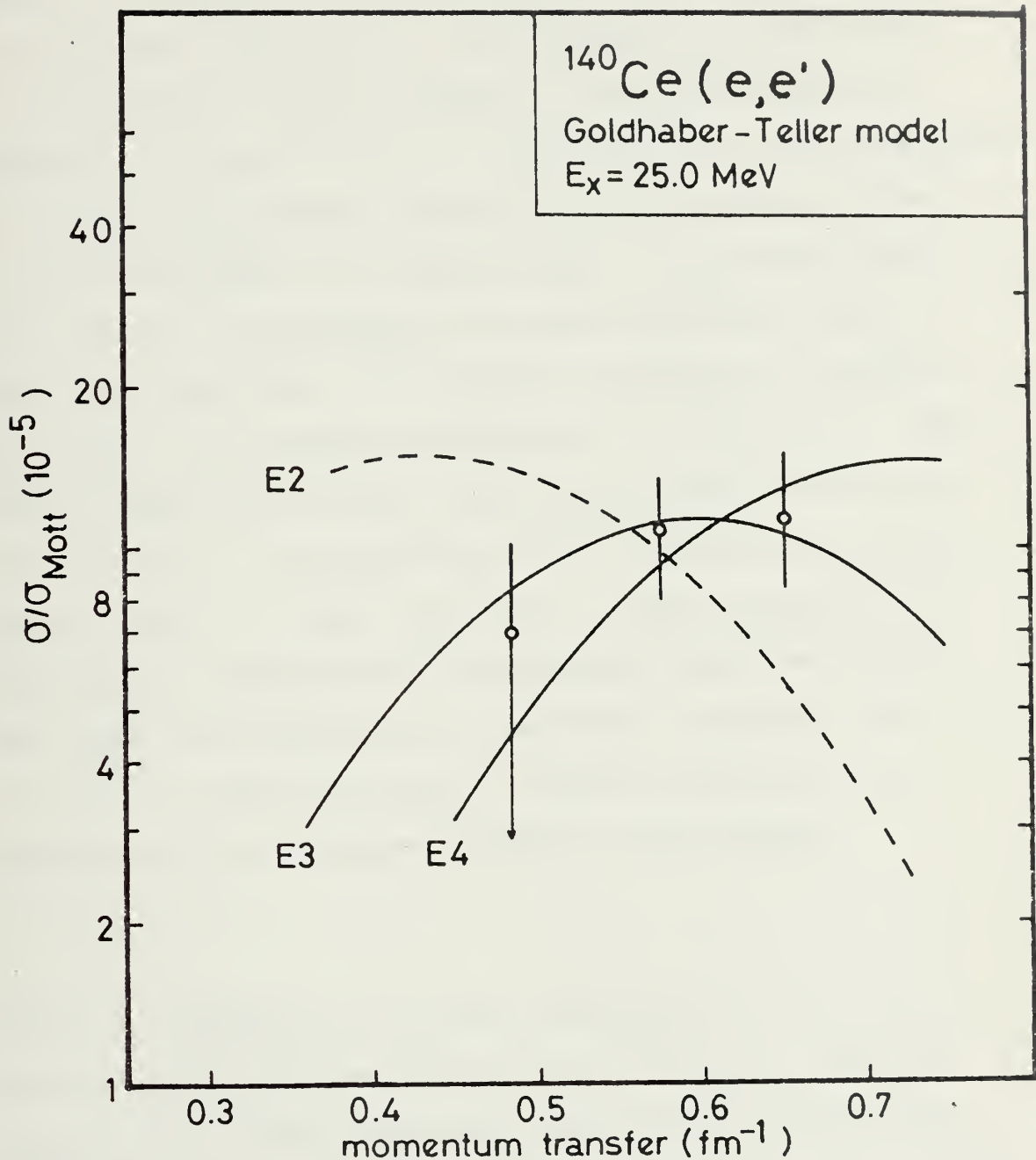


FIGURE 12. Comparison of the difference between the experimental and the DWBA form factors for the resonance found at 25.0 MeV.

## FIGURE CAPTIONS

Figure 1. Spectrum of 92.1 MeV electrons scattered inelastically from  $^{140}\text{Ce}$  at  $90^\circ$ . The spectrum with and without the background is shown together so that the difference between the two may be seen. The resonances which were used for fitting the spectrum and the background as described in the text are drawn. The "ghost peak" is subtracted from both graphs. The spectrum was taken and fitted with 10 data points per MeV. For graphical purposes the number of points for the spectrum was reduced by a factor of 4. The fitting range was 4-48 MeV; the broken lines are drawn to guide the eye. The statistical error is shown on selected points. While the upper part has not been corrected for the constant dispersion of the magnetic spectrometer and thus shows the data points as measured, the subtracted spectrum has been corrected, in order to show the cross sections of the resonances in their true relation.

Figure 2. Spectra of 79.6 MeV electrons and 92.8 MeV electrons scattered inelastically from  $^{140}\text{Ce}$  at  $90^\circ$  and  $105^\circ$  respectively. The spectra were taken and fitted with 10 data points per MeV. For graphical purposes the number of points was reduced by a factor of 4. The fitted range was 4-48 MeV; the statistical error is shown on selected points.

Figure 3. Spectra of 79.6 MeV electrons and 92.8 MeV electrons scattered inelastically from  $^{140}\text{Ce}$  at  $90^\circ$  and  $105^\circ$  respectively. The fitted background (consisting of the radiation tail and the general room background) and the "ghost peak" as described in the text have been subtracted. These two spectra are shown together so that the shrinkage of smaller multipolarity transitions versus the growth of higher multipolarity transitions may be seen. The relative change in peak heights of the single resonances indicate very clearly the various multipoles contributing. Note, e.g., that the E2 cross sections fall off more than a factor of 6 between the 80/90 and the 90/105 spectra.

Figure 4. The photon absorption cross section of  $^{140}\text{Ce}$ . The data are from experiments conducted at Saclay (LepB 76).

Figure 5. Comparison of DWBA cross sections for E1 to E4 transitions divided by the Mott cross sections. The curves are interpolations between calculations for the correct energy and angle of the five measurements used, since the data in this work and from Pitthan (Pit 73) vary greatly in electron beam energy. The curves were normalized so that the first maxima are equal. The program of Tuan et al. (TuaW 68) was used with a transition charge density  $\rho_{tr}(r) = N_\lambda r^\lambda d\rho_0(r)/dr$ .

Figure 6. Comparison of the DWBA and experimental form factors for the resonance found at 15.3 MeV. The experimental form factors are compared to the Goldhaber-Teller, Steinwedel-Jensen and Myers-Swiatecki models. The mixed model of Myers, Swiatecki et al. (MyeS 77), explained in the text, fits the experimental data best. A mixture ratio, based on the drop-let model, of 0.76 was used. The curves are not fitted to the  $(e, e')$  data, but to the photon measurement of Figure 4.

Figure 7. Comparison of the difference between the experimental form factors and the Goldhaber-Teller model (see Figure 6) and the DWBA form factors for the resonance found at 15.3 MeV. The difference shows that the possibility of an E0 transition with  $45 \pm 15\%$  of the monopole isoscalar sum rule lying beneath the dipole exists if the Goldhaber-Teller model is assumed to be correct.

Figure 8. Comparison of the DWBA and experimental form factors for the resonance found at 12.0 MeV. The Goldhaber-Teller model for an E2 transition was fit to the experimental data first using as the half density radius  $c_{tr} = c$  and second as  $c_{tr} = 0.95 c$  as explained in the text.

Figure 9. Comparison of the difference between the experimental form factor and the Goldhaber-Teller model DWBA form factor with  $c_{tr} = c$  (see Figure 8) for the resonance found at 12.0 MeV. The difference shows that an E3 transition beneath the E2 transition found at 12.0 MeV exists if the

Goldhaber-Teller model is assumed to be correct. An E4 transition lying beneath the resonance at 12.0 MeV may be ruled out.

Figure 10. Comparison of the DWBA and experimental form factors for the resonances found at 6.0, 7.4, and 10 MeV. The Goldhaber-Teller model for an E3 transition fits the experimental form factors of the 6.0 MeV resonance, while an E2 or E4 assignment of form factors can clearly be ruled out. The Goldhaber-Teller model for an E3 transition best fits the experimental form factors for the resonance found at 7.4 MeV; however, an E4 transition cannot be ruled out. An E2 assignment of the form factor, though, can be clearly ruled out. The Goldhaber-Teller model for an E2 (E0) transition fits the experimental form factors of the resonance found at 10.0 MeV. The assignment of an E1 or an E3 transition can be ruled out.

Figure 11. Comparison of the DWBA and experimental form factors for the resonances found at 22.0, 25.0, 31.0 and 37.5 MeV. The Goldhaber-Teller model for an E3 transition fits the experimental form factors of the resonance found at 22.0 MeV. An E2 or an E4 assignment of form factors can be ruled out. Both the Goldhaber-Teller and the Myers-Swiatecki E2 models were fit to the experimental form factors for the resonances found at 25.0 MeV. The Myers-Swiatecki model with a mixture ratio of 1.0 was found to fit the data

better than the Goldhaber-Teller model as explained in the text. The assignment of an E3 transition can be clearly ruled out. The experimental form factor of the resonance found at 31.0 MeV fit the Goldhaber-Teller model for both E3 and E4 transitions. An upper value could only be estimated for the form factor obtained from the 80/90 experiment as explained in the text. The assignment of an E2 transition can be clearly ruled out. The Goldhaber-Teller model for an E3 transition fits the experimental form factors for the resonance found at 37.5 MeV. An E2 assignment can be clearly ruled out, but a sizeable E4 contribution seems possible.

Figure 12. Comparison of the difference between the experimental form factors and the Goldhaber-Teller model (see Figure 11) and the DWBA form factor for the resonance found at 25.0 MeV. The difference shows that the possibility of an E3 or an E4 transition lying beneath the E2 transition exists if the Goldhaber-Teller model is assumed to be correct.

LIST OF REFERENCES

BeaK 77 Beachy, J.S., Kowalick, S.J. Jr: M.S. Thesis, Naval Postgraduate School, March 1977 (unpublished).

Ber 76 Berman, B.L., Atlas of Photoneutron Cross Sections Obtained with Monoenergetic Photons, Lawrence Livermore Lab., Livermore, Ca. December 1976, Preprint UCRL-78482.

BerK 69 Berman, B.L., Kelly, M.A., Bramblett, R.L., Caldwell, J.T., Davis, H.S., Fultz, S.C., Phys. Rev., 185, 1576 (1969).

BohM 75 Bohr, A. and Mottelson, B.R.: Nuclear Structure, V. 2, W.A. Benjamin Inc., Reading Massachusetts.

BorK 75 Borzov, I.N. and Kamerdzhev, S.P.: Yad. Fiz. 21, 31 (1975) [Sov. J. Nucl. Phys. 21, 15 (1975)].

FerW 74 Ferlic, K.P.; Waddell, R.D.: M.S. Thesis, Naval Postgraduate School, June 1974 (unpublished).

FisR 64 Fischer, C.R., and Rawitscher, G.H.: Phys. Rev., 135, B377 (1964).

FukT 76 Fukuda, S. and Torizuka, Y.: Phys. Lett. 62B, 146 (1976).

GinP 64 Ginsberg, E.S. and Pratt, R.H.: Phys. Rev., 134, 4, B773 (1964).

GolT 48 Goldhaber, M. and Teller, E.: Phys. Rev., 74, 1046 (1948).

Gor 75 Gordon, E.F.: M.S. Thesis, Naval Postgraduate School, December 1975 (unpublished).

GorP 77 Gordon, E.F.; Pitthan, R., Nucl. Instr. Meth. 145, 569 (1977).

Ham 72 Hamamoto, J. in Proceedings of the International Conference on Nuclear Structure Studies Using Electron Scattering and Photoreaction, Sendai, 1972, edited by K. Shoda and H. Ui [Suppl. Res. Rep. Nucl. Sci., Tohoku Univ., 5, 205 (1972)].

HicA 77 Hicks, R.S.; Auer, J.P.; Bergstrom, J.C., Caplan, H.S.; Nuclear Physics A278, 261 (1977).

HouM 77 Houk, A.H.; Moore, R.W.: M.S. Thesis, Naval Postgraduate School, March 1977 (Unpublished).

KawK 68 Kawai, M. and Kikuchi, K., Nuclear Matter and Nuclear Reactions, North-Holland Publishing Co., Amsterdam (1968).

KreS 74 Krewald, S. and Speth, J.: Phys. Lett. 52B 295 (1974).

LepB 76 Leprêtre, R.; Beil, H.; Bergère, R.; Carlos, P.; Fagot, J.; de Miniac, A.; Veyssiére, A.; Miyase, H.: Nucl. Phys. A258, 350 (1976).

LiuB 76 Liu, K.F.; Brown, G.E.; Nuclear Physics A265, 385 (1976).

Mig 44 Migdal, A.: J. Phys. USSR 8, 331 (1944).

Mon 69 Moniz, E.J., Phys. Rev. 184, 1154 (1969).

MonS 71 Moniz, E.J.; Sick, I.; Whitney, R.R.; Ficenec, J.R.; Kephart, R.D.; Trower, W.P., Phys. Rev. Lett. 26, 445 (1971).

MooB 76 Moore, G.L.; Buskirk, F.R.; Dally, E.B.; Dyer, J.N.; Maruyama, X.K.; Pitthan, R; Z. Naturforsch., 31a, 668 (1976).

MosY 76 Moss, J.M.; Youngblood, D.H.; Rozsa, C.M.; Brown, D.R. and Bronson, J.D.; Phys. Rev. Lett. 37, 13 (1976).

Mye 74 Myers, W.D.: Lawrence Berkely Laboratory Report No. LBL-3428, Nov. 1974 (unpublished).

MyeS 69 Myers, W.D.; Swiatecki, W.J.: Ann. Phys. (N.Y.) 55, 395 (1969).

MyeS 73 Myers, W.D.; Swiatecki, W.J.: Ann. Phys. (N.Y.) 84, 186 (1973).

MyeS 77 Myers, W.D. and Swiatecki, W.F.; Kodama, T. and El-Jaick, L.J.; Hilf, E.R.: Phys. Rev., 15, 2032 (1977).

Pit 73 Pitthan, R.; Z. Phys. 260, 283 (1973).

PitB 74 Pitthan, R., Buskirk, F.R., Dally, E.B., Dyer, J.R., and Maruyama, X.K.: Phys. Rev. Letters, 33, 849 (1974).

PitB 77 Pitthan, R., Buskirk, F.R., Dally, E.B., Shannon, J.O. and Smith, W.H.: Phys. Rev. 16, 970 (1977).

PitW 71 Pitthan, R. and Walcher, T.: Phys. Letters, 36B, 563 (1971).

Ric 77 Richter, A., in Proceedings of the Sendai Conference on Electro- and Photoexcitations, Sendai, 1977, edited by Y. Kawazoe; p. 195.

Sch 76 Schwierczinski, A., Untersuchung der El- und isokalaren E2 - Riesenresonanz von  $^{142}\text{Nd}$  und  $^{150}\text{Nd}$  mit unelastischer Electronenstreuung, Ph.D. Thesis, Techn, Hochschule Darmstadt, West Germany, 1976.

SteJ 50 Steinwedel, H. and Jensen, J.H.D.: Z. Naturforsch 5a, 413 (1950).

Tas 56 Tassie, L.J.; Austral. J. Phys. 9, 407 (1956).

The 72 Theissen, H.: Springer Tracts in Modern Physics Vol. 65, Springer-Verlag, Berlin, 1972.

Tho 69 Thompson, A. Ch.: Ph.D. Thesis Carnegie-Mellon-University, Pittsburgh (1969); Report CAR-882-24.

TuaW 68 Tuan, S.T.; Wright, L.E.; Onley, D.S.: Nuclear Instruments and Methods, 60, 70, (1971).

Übe 71 Überall, H.: Electron Scattering from Complex Nuclei, V. 2, Academic Press, 1971.

WarW 69 Warburton, E.K. and Wenesser, J.: The Role of Isospin in Electromagnetic Transitions, ed. by Wilkinson, D.H., North-Holland Publishing Company, Amsterdam, 1969.

YouR 77 Youngblood, D.H., Rozsa, C.M.; Moss, J.M., Brown, D.R., and Bronson, J.D.: Phys. Rev. Lett. 39, 19 (1977).

ZieP 68 Ziegler, J.F. and Peterson, G.A.: Phys. Rev., 165, 1337 (1968).

INITIAL DISTRIBUTION LIST

	No. Copies
1. Defense Documentation Center Cameron Station Alexandria, Virginia 22314	2
2. Library, Code 0142 Naval Postgraduate School Monterey, California 93940	2
3. Department Chairman, Code 61 Department of Physics and Chemistry Naval Postgraduate School Monterey, California 93940	2
4. Professor F.R. Buskirk, Code 61Bs Department of Physics and Chemistry Naval Postgraduate School Monterey, California 93940	3
5. Professor R. Pitthan, Code 61Pt Department of Physics and Chemistry Naval Postgraduate School Monterey, California 93940	2
6. Professor J.N. Dyer, Code 61Dy Department of Physics and Chemistry Naval Postgraduate School Monterey, California 93940	1
7. LCDR Hubert Hass Lessingstrasse 10 2400 Luebeck Federal Republic of Germany	1
8. LT. D.H. Meyer 133 N. Chestnut Street Bath, Pennsylvania 18014	1
9. Marineamt -Al- 2940 Wilhelmshaven Federal Republic of Germany	1
10. Dokumentationszentrale der Bundeswehr (See) Friedrich-Ebert-Allee 34 5300 Bonn Federal Republic of Germany	1

thesH31225  
Electroexcitation of giant resonances be



3 2768 002 07786 9

DUDLEY KNOX LIBRARY